# THE UNDERSTANDING SEVERE THUNDERSTORMS AND ALBERTA BOUNDARY LAYERS EXPERIMENT (UNSTABLE) 2008

BY NEIL M. TAYLOR, DAVID M. L. SILLS, JOHN M. HANESIAK, JASON A. MILBRANDT, CRAIG D. SMITH, GEOFF S. STRONG, SUSAN H. SKONE, PATRICK J. MCCARTHY, AND JULIAN C. BRIMELOW

A field and modeling study aims to improve our understanding of boundary layer processes in the foothills of the Alberta Rocky Mountains and how they relate to the initiation of severe thunderstorms.

**Understanding convective initiation (CI) and predicting severe thunderstorms remains a challenge for atmospheric scientists and forecasters. However, accurate forecasts of the timing and location of CI are critical to maximize the lead time and accuracy of severe weather watches and warnings. The small spatial and temporal scales (sometimes only hundreds of meters and minutes, respectively) on which atmospheric processes leading to CI occur make them difficult to measure observationally and simulate using numerical weather prediction (NWP) models. An attempt to resolve these processes via observations can be made using ▶**

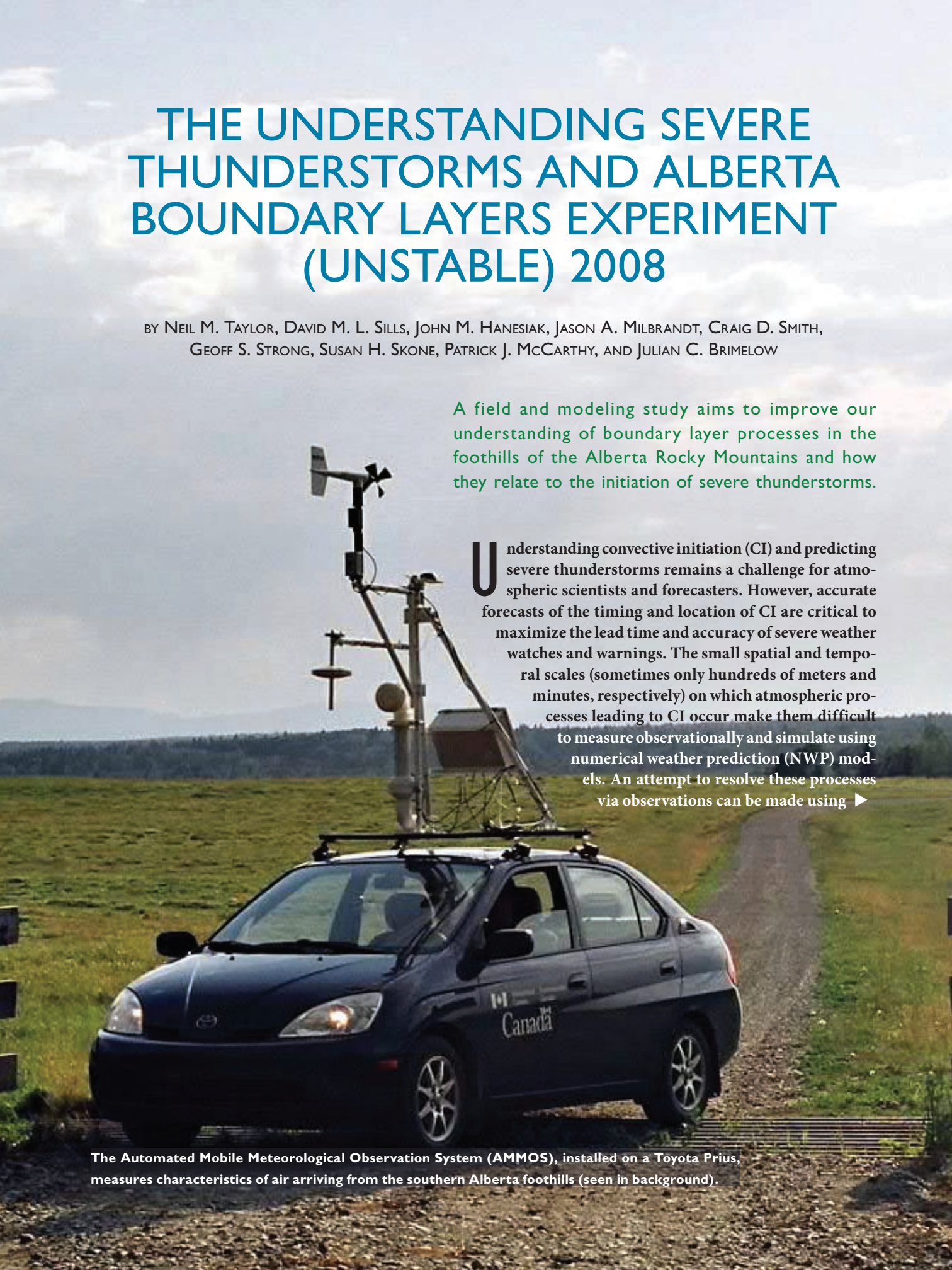


**The Automated Mobile Meteorological Observation System (AMMOS), installed on a Toyota Prius, measures characteristics of air arriving from the southern Alberta foothills (seen in background).**

targeted field measurements in active thunderstorm regions.

In Canada, one of the most active regions for severe thunderstorm activity is the Canadian prairies. On average, 221 severe[1] events are reported to Environment Canada (EC) over the prairies each summer (McDonald 2009). A recognized genesis region for storms on the western prairies is the mountain–prairie transition zone along the front range of the Rocky Mountains known as the foothills region of Alberta, Canada. This area is typically associated with more lightning days than anywhere else on the prairies (Fig. 1). Storms developing over the foothills generally move eastward to affect the Edmonton–Calgary corridor, one of the most densely populated and fastest-growing regions in Canada (Statistics Canada 2007). Since 1981, Public Safety Canada estimates that more than 40 deaths and $2.5 billion (Canadian dollars) in damage can be attributed to severe thunderstorms in Alberta (see Table 1). Typically, the most damaging storms are supercells with large hail and/or tornadoes.

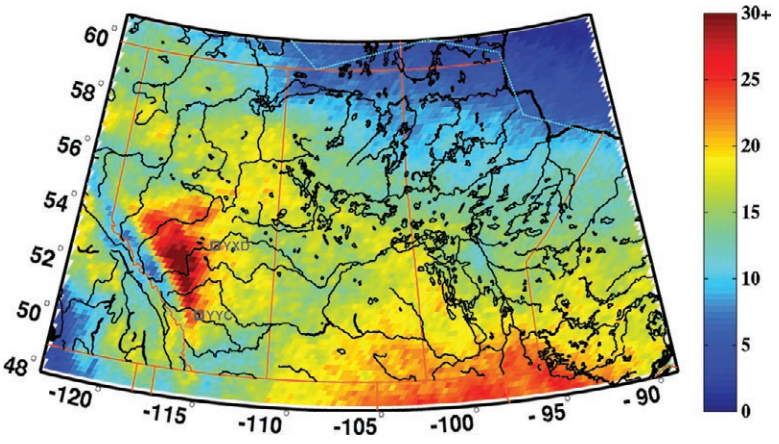


**Fig. 1. Average number of days (1–30 Sep) between 1999 and 2008 with at least one cloud-to-ground lightning flash over the Canadian prairies. The cities of Edmonton (YXD) and Calgary (YYC) are indicated. Data from the CLDN (W. R. Burrows 2009, personal communication).**

Requests from forecasters, and the potential for future losses, prompted the design of a field experiment to investigate CI over the Alberta foothills. UNSTABLE (refer to Table 2 for acronym expansion) was designed to take place over two summers. In 2008, a pilot experiment was conducted to collect observations and test measurement strategies for a later full-scale experiment. The overall goal of UNSTABLE is to improve our understanding of processes associated with CI and to work with forecasters to maximize severe thunderstorm watch and warning lead times and accuracy. UNSTABLE has been designed to examine CI processes as opposed to targeting a particular type of event (e.g., storms producing large hail). Forecaster assessment of the prestorm environment should identify likely convective mode and associated severe weather elements. A better understanding of how, when, and where storms may form should support more informed watch and warning decisions prior to the occurrence of severe weather from a parent storm.

This article provides the rationale for developing UNSTABLE and general information on the design and operations of the 2008 pilot campaign. Preliminary results from 2008 will illustrate how UNSTABLE observations will be used to learn more about CI processes in Alberta. We begin with a discussion of challenges associated with forecasting CI and a review of Canadian thunderstorm research focused mainly in Alberta. This is followed by an

**AFFILIATIONS:** Taylor—Hydrometeorology and Arctic Lab, Environment Canada, Edmonton, Alberta, Canada; Sills—Cloud Physics and Severe Weather Research Section, Environment Canada, Toronto, Ontario, Canada; Hanesiak and Brimelow—Department of Environment and Geography, Centre for Earth Observation Science, University of Manitoba, Winnipeg, Manitoba, Canada; Milbrandt—Numerical Weather Prediction Research Section, Environment Canada, Dorval, Quebec, Canada; Smith—Climate Research Division, Environment Canada, Saskatoon, Saskatchewan, Canada; Strong—Department of Earth and Atmospheric Sciences, University of Alberta, Edmonton, Alberta, Canada; Skone—Department of Geomatics Engineering, University of Calgary, Calgary, Alberta, Canada; McCarthy—Prairie and Arctic Storm Prediction Centre, Environment Canada, Winnipeg, Manitoba, Canada
**CORRESPONDING AUTHOR:** Neil M. Taylor, Environment Canada, 4999 98th Ave., Room 200, Edmonton AB T6B 2X3, Canada
E-mail: neil.taylor@ec.gc.ca

*The abstract for this article can be found in this issue, following the table of contents.*
DOI:10.1175/2011BAMS2994.1

In final form 21 January 2011


[1] In Alberta, severe thunderstorm event criteria are tornadoes, hail diameter ≥20 mm, wind gusts ≥90 km $h^{-1}$, and/or convective rainfall amounts of ≥50 mm in one hour.

**Table 1. List of the costliest Alberta summer severe weather events from 1981 to 2008. All values taken from Public Safety Canada's Canadian Disaster Database (www.publicsafety.gc.ca/prg/em/cdd/srch-eng.aspx). Dollar figures for events prior to 2001 have been adjusted to 1999 Canadian dollars. Events in bold resulted in loss of life or at least $100 million in estimated losses.**

| Date | Location | Event | Estimated damage ($) | Deaths |
|---|---|---|---|---|
| **7 Sep 1991** | **Calgary** | **Hail** | **884,595,000** | 0 |
| **31 Jul 1987** | **Edmonton** | **Tornado/hail** | **665,483,000** | **27** |
| **16–18 Jul 1996** | **Calgary** | **Hail** | **305,854,000** | 0 |
| **28 Jul 1981** | **Calgary** | **Hail** | **288,414,000** | **2** |
| 24–25 Jul 1996 | Calgary | Hail | 87,877,000 | 0 |
| 17 Jul 1995 | Calgary | Hail | 74,559,000 | 0 |
| 11 Jul 2004 | Edmonton | Hail | 74,000,000 | 0 |
| 4–8 Jul 1998 | Calgary | Hail | 65,258,000 | 0 |
| 16 Aug 1988 | Calgary | Hail | 61,024,000 | 0 |
| 3 Jul 1991 | Red Deer | Hail | 40,387,000 | 0 |
| 31 Jul 1992 | Calgary | Hail | 38,495,000 | 0 |
| 4 Jul 1995 | Edmonton | Hail | 34,511,000 | 0 |
| 18 Jun 1994 | Southern Alberta | Hail | 30,969,000 | 0 |
| **14 Jul 2000** | **Pine Lake** | **Tornado/hail** | **30,477,000** | **12** |
| 1 Sep 1992 | Edmonton | Hail | 22,522,000 | 0 |
| 9 Jul 1990 | Calgary | Hail | 22,028,000 | 0 |
| 29 Jul 1993 | Edmonton | Hail | 21,095,000 | 0 |
| 28 Aug 1992 | Edmonton | Hail | 20,170,000 | 0 |
| **Total estimated cost** | | | 2,767,718,000 | 41 |

outline of UNSTABLE goals and experimental design and selected observations from the 2008 campaign. We conclude with a summary discussion outlining future UNSTABLE-related research.

**CI FORECAST CHALLENGES.** Results from studies in Alberta (Taylor 1999) and on the U.S. high plains (Mueller et al. 1993) suggest that stability of the mid–upper troposphere ranges from neutral to conditionally unstable on most days during the warm convective season. The potential for CI is modulated by the environmental lapse rate above the level of free convection (LFC), so that sufficient instability is required to counter the effects of parcel dilution during ascent (Houston and Niyogi 2007). When such a condition exists, the potential for CI is additionally influenced by atmospheric boundary layer (ABL) thermodynamic and kinematic processes (Mueller et al. 1993). ABL processes associated with water vapor availability and depth (Mueller et al. 1993; Crook 1996; Weckwerth and Parsons 2006), the presence of convergence lines (Wilson and Schreiber 1986; Wilson and Mueller 1993; Sills et al. 2002, 2004; King et al. 2003; Wilson and Roberts 2006), or mesoscale circulations and interactions with boundaries (Weckwerth and Wakimoto 1992; Kingsmill 1995; Sills et al. 2004; Buban et al. 2007) have been found to contribute to CI. The strength and evolution of convective inhibition (CIN) in response to synoptic or mesoscale lift or other factors further influence the potential for CI (Strong 1986; Browning et al. 2007). Additional studies (Doran et al. 1995; Weaver and Avissar 2001; Raddatz and Cummine 2003; Hanesiak et al. 2004; Trier et al. 2004) suggest that the above processes can be influenced by the heterogeneity of surface characteristics related to soil moisture and vegetation cover. Results from these and other studies imply that the effects of ABL convergence and water vapor availability (and depth) on the potential for CI are linked. For forecasts of CI to improve, these processes need to be more completely observed and understood. In recent years, several field studies with CI research components have been conducted worldwide (see Table 2) in regions with varying degrees of orography and convective instability. UNSTABLE targets the transition area between the

**Table 2. Recent field studies with a CI component. QPF means quantitative precipitation forecast.**

| Name | Acronym | Field campaigns | Location | Orography/ influence | Foci | References |
|---|---|---|---|---|---|---|
| Effects of Lake Breezes on Weather | ELBOW | 1997, 2001 | Southern Ontario, Canada | Minor orography, lake breezes | CI and severe storms in association with lake breezes | King and Sills (1998); Sills et al. (2002) |
| The International $H_2O$ Project 2002 | IHOP_2002 | 2002 | Southern Great Plains, United States | Minor orography | ABL water vapor processes and observations, CI, and QPF | Weckwerth et al. (2004) |
| The Convective Storm Initiation Project | CSIP | 2004, 2005 | Southern England | Moderate orography, coastal influence | Location and timing of CI and improved NWP | Browning et al. (2007) |
| The Cumulus Photogrammetric, In Situ, and Doppler Observations | CuPIDO | 2006 | Santa Catalina Mountains, Arizona, United States | Transition from desert plains to mountains | CI and cumulus dynamics | Damiani et al. (2008) |
| The Convective and Orographically Induced Precipitation Study | COPS | 2007 | Southwest Germany and eastern France | Complex and mountainous | CI and QPF | Wulfmeyer (2008) |
| The Understanding Severe Thunderstorms and Alberta Boundary Layers Experiment 2008 | UNSTABLE | 2008, 2013 (proposed) | Rocky Mountain foothills, Alberta, Canada | Transition from mountains to plains | CI and severe storms associated with mesoscale boundaries, land surface processes, and NWP | Taylor et al. (2008b) |

Rocky Mountains to the west and agricultural prairie regions to the east. Here, differential heating of terrain and upper-flow interactions with the mountain barrier can create local mesoscale boundaries and circulations that influence CI (e.g., Smith and Yau 1993a,b). The prestorm environment in this region is frequently characterized by weak CIN, moderate convective instability, and moderate-to-strong deep-layer wind shear (Strong 1986).

Observational (Mueller et al. 1993) and modeling (Crook 1996) studies have indicated that horizontal variations of surface water vapor mixing ratio ($q_v$) and potential temperature ($\theta$) of 1 g kg$^{-1}$ and 1 K, respectively, can mean the difference between no deep moist convection and intense thunderstorms. Such variability often occurs on scales that are much smaller than can be resolved with existing synoptic-scale observation networks (Mueller et al. 1993; Crook 1996). Water vapor depth in the ABL has also been shown to critically affect CI, as storms appear to be favored in areas with deeper ABL moisture (Mueller et al. 1993; Weckwerth et al. 1996; Weckwerth 2000; McCaul and Cohen 2002). Small horizontal changes in temperature and water vapor, and vertical changes in moisture depth, can significantly affect assessments of static stability (Crook 1996; Bunkers et al. 2002; Craven et al. 2002) needed to identify areas with potential for CI.

Observations of near- and above-surface variability in thermodynamic parameters (e.g., $q_v$ and $\theta$) and wind are required to understand how, and why, CI occurs. In Canada, the existing observational network was designed to resolve synoptic-scale features, and it generally does not allow for detailed observations of mesoscale processes. For Alberta forecasters, there is one upper-air station 40 km west of Edmonton at Stony Plain (53.55°N, 114.10°W; Fig. 2). Soundings from this station are approximately 200 km from where storms are observed to form over the foothills and are often not representative of ABL characteristics in that region (Strong 1986; Taylor 1999). At the surface, observations of mesoscale processes associated with CI require measurements with high spatial and temporal resolution. However, real-time observations over the foothills are limited, with a significant void in surface observations where storms typically form (see Fig. 2 for existing real-time hourly surface observation locations available to forecasters). Targeted observations obtained through field studies offer an opportunity to augment data-poor areas and

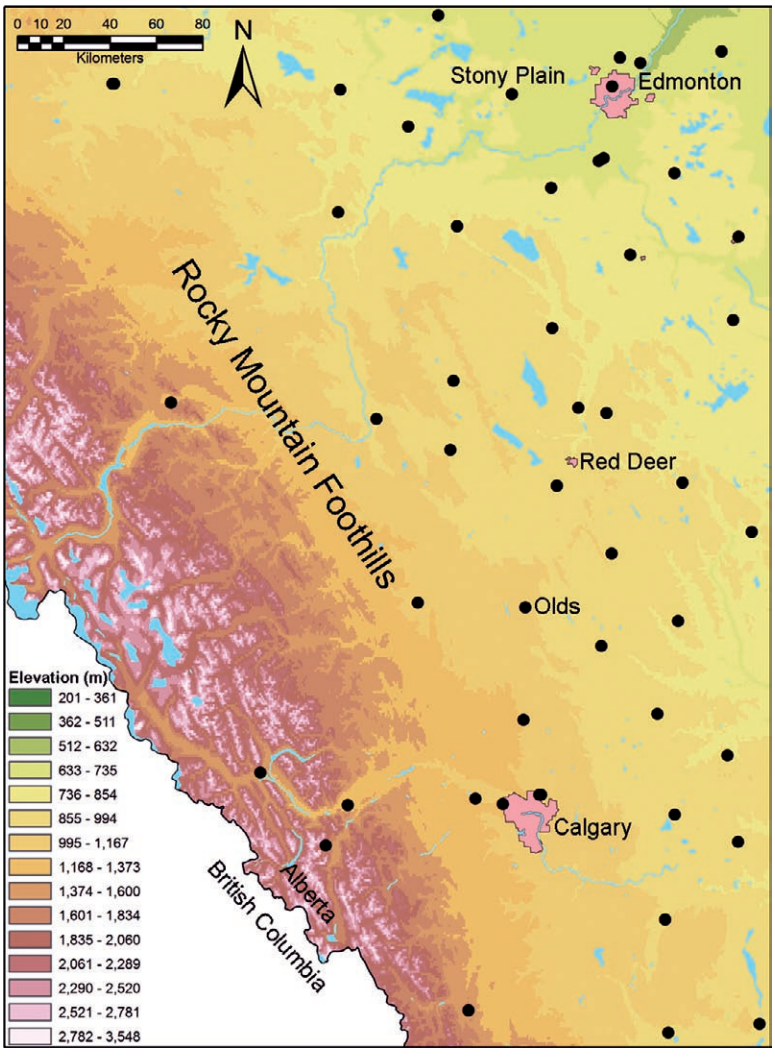


**Fig. 2. Relief map showing the Edmonton–Calgary corridor, the Stony Plain upper-air station, and existing real-time surface observation locations available to forecasters (black circles). The foothills region is characterized by the transition from lower-lying agricultural areas (east) to the Rocky Mountains (west). Very few real-time surface observations are available over the Alberta foothills.**

collect measurements more suitable for resolving mesoscale processes.

## ALBERTA THUNDERSTORM RESEARCH.

There is a rich history of thunderstorm research in Alberta dating back to the Alberta Hail Studies Project (Wojtiw 1975) beginning in 1956. Research related to severe storm outbreaks was conducted by Longley and Thompson (1965), who constructed mean maps for hail and no-hail days using upper-air sounding data. Research in the 1970s focused on hail observations and modeling (Chisholm 1973; English 1973; Renick and Maxwell 1977) and storm-scale studies, including kinematic models for single cell, multicell, and supercell hailstorms pioneered by Chisholm and Renick (1972). A conceptual model for convective outbreaks in Alberta was developed based on observations from the 1979 Severe Environmental Storms and Mesoscale Experiment (SESAME) in the United States and the 1980–85 Limestone Mountain Experiment (LIMEX) in Alberta (Strong 1986, 1989). This model describes how the approach of an upper trough, an increase in CIN, the development of upslope flow, and the subsequent reduction of CIN through orographic and synoptic lift with trough passage leads to severe weather outbreaks. Using LIMEX-85 data, Honch and Strong (1990) noted a line of surface convergence associated with CI, hinting at the importance of mesoscale boundaries for CI in this region. A later modification of this model (Smith and Yau 1993a,b) focused on the development of a mountain–plain circulation contributing to moisture transport from the plains to the foothills.

A number of the above-mentioned studies recognized the importance of mesoscale and ABL processes for CI. Specific emphasis on surface boundaries with respect to moisture and convergence was discussed by Knott and Taylor (2000), who referred to an observed moisture and convergence boundary as a dryline using limited operational surface and remote sensing observations. Hill (2006) showed the first mobile surface observations and moisture gradients collected across the dryline in Alberta. These studies illustrated the inadequacy of the existing operational network to explicitly resolve the dryline at the surface.

The Canadian prairies are far removed from the Gulf of Mexico, the primary source of ABL water vapor on the U.S. Great Plains. Consequently, Canadian researchers and forecasters have long recognized the importance of evapotranspiration (ET) as a local, or upstream, moisture source contributing to the potential for CI and severe storms. The influence of soil moisture and sensible and latent heat

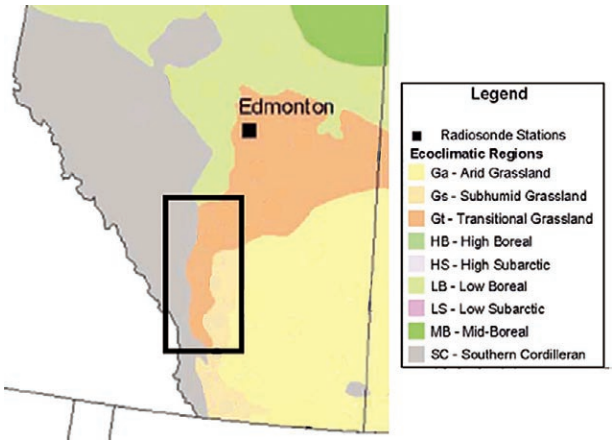


**Fig. 3. Ecoclimatic regions of southern Alberta. The black rectangle indicates the area with significant changes in ecoclimatic region described in the text. The square near Edmonton represents the EC Stony Plain radiosonde station (adapted from Raddatz and Noonan 2004).**

fluxes on ABL evolution has been well established (Entekhabi et al. 1996; Pielke 2001). ET has been proposed as an important source of ABL water vapor for CI and moisture recycling on the Canadian prairies (Strong 1997; Raddatz 1998, 2000, 2005; Raddatz and Cummine 2003; Hanesiak et al. 2004). The Alberta foothills are in close proximity to a transition zone in ecoclimate regions between southern cordilleran and prairie grasslands to the east (Fig. 3). ET from prairie crops and grasslands are a potential source of ABL water vapor that may be advected into the foothills region to promote CI.

Modeling studies of severe storms in Alberta (e.g., Erfani et al. 2003; Milbrandt and Yau 2006a,b) have reproduced supercell-like structures consistent with radar observations, and they have shown a potential to provide useful guidance to forecasters with respect to CI and storm evolution. Computational power is now available to run NWP models at high spatial resolution (e.g., 1-km horizontal grid spacing) in real time. In addition to comparing storm and precipitation pattern forecasts, model simulations of the physical processes associated with CI need to be considered.

**UNSTABLE GOALS AND EXPERIMENTAL DESIGN.** The goals of UNSTABLE are as follows:

- To better understand atmospheric processes leading to thunderstorm development over the Alberta foothills (both prior to and during CI) with an aim to extend results elsewhere in Canada
- To improve accuracy and lead time for severe thunderstorm watches and warnings
- To assess the skill of a high-resolution model to resolve physical processes over the Alberta foothills and to assess its utility for providing useful numerical guidance for the forecasting of severe convection
- To refine through observational, case, and numerical modeling studies existing conceptual models describing CI and the development of severe thunderstorms over Alberta and the western prairies.

UNSTABLE was designed following three main themes posed in the form of overarching science questions (Q1–Q3) [see Taylor et al. (2007) for further details].

*Q1.* What are the contributions of ABL processes to the initiation of deep moist convection and the development of severe thunderstorms in the Alberta foothills region?

Q1 deals with ABL water vapor availability and stratification in the vertical, the role of mesoscale boundaries and circulations in CI, the four-dimensional characterization of the dryline, factors inhibiting CI, and the revision of existing conceptual models for CI in this region.

*Q2.* What are the contributions of surface processes to the initiation of deep moist convection and the development of severe thunderstorms in the Alberta foothills region?

Q2 seeks primarily to investigate the effects of root-zone soil moisture and associated vegetation condition on the ABL and their relation to local CI processes. These include the development of horizontal water vapor gradients, mesoscale circulations, and resulting axes of moisture and mass convergence in response to contrasting areas of root-zone soil moisture and vegetation type. During the pilot project, observations were limited to meteorological measurements with no direct latent and sensible heat measurements.

*Q3.* To what extent can high-resolution NWP models contribute to forecasting the initiation and development of severe convective storms that originate in the Alberta foothills?

Q3 targets the use of NWP models in forecasting CI and severe storms. Investigations include examining the skill of the Canadian Global Environmental Multiscale (GEM) model (Côté et al. 1998), run at the convective

scale, to simulate ABL and surface processes under consideration in Q1 and Q2. Observed storm structures, microphysical fields, and potential deficiencies in current parameterizations will also be examined.

These three questions formed the basis for the design of a 2008 pilot field campaign. The experimental domain and study period, special instrumentation used, and measurement strategies were defined to address the three above-mentioned questions while exploiting existing observational infrastructure. Additional consideration was given to known spatial and temporal characteristics of thunderstorm activity in Alberta. Dedicated convective-scale NWP support was designed to support all three science questions utilizing both conventional and experimental forecast fields over an appropriate domain and forecast period. The model runs were conducted in real time to support field operations.

*Experimental domain.* The experimental domain for UNSTABLE (Fig. 4) was defined using criteria including thunderstorm activity, proximity to population centers, and existing observational infrastructure. The domain encompasses the southern half of the climatological maximum for thunderstorm days (Fig. 1) and days with hail (Wojtiw 1975; not shown) in Alberta and is a region long recognized for frequent CI and severe weather in summer. Given the impact of severe storms on population centers, the domain was defined to include the cities of Calgary and Red Deer. The contrasting region of crops/grasslands and forests (Fig. 3) and the presence of research monitoring networks [e.g., Foothills Orographic Precipitation Experiment (FOPEX) and Foothills Climate Array (FCA), see Table 3] helped further refine the UNSTABLE domain. A subdomain was defined to target CI processes over the foothills specifically and to include the majority of special fixed instrumentation and mobile observations. This included two lines of mesonet stations (M1–M8 in Fig. 4) with varied spacing oriented along the sloping terrain of the foothills.

*Instrumentation and observations.* A summary of special instrumentation deployed/utilized for UNSTABLE 2008 is provided in Table 3. Fixed networks of surface stations, GPS precipitable water (PW) sensors, two rawinsonde stations, a water vapor radiometer (WVR), a water vapor profiler (WVP), and a tethersonde provided stationary surface and upper-air observations within the UNSTABLE domain. On selected days, additional mobile platforms consisting of 1–3 instrumented vehicles (IV1–IV3), two rawinsonde stations [mobile balloons 1 and 2 (MB1 and MB2, respectively)], instrumented aircraft, and an integrated profiling system [Atmospheric Emitted Radiance Interferometer (AERI), infrared pyrometer, and WVR] were deployed to specific target areas. Additionally, the IV2 team placed Styrofoam "hail pads" at roadside locations with 2–5-km spacing. The pads were calibrated to record hail size and impact energy and were collected and replaced after hail occurred.

Data from the operational networks used by EC forecasters [e.g., C-band Doppler radars, *Geostationary Operational Environmental Satellite 12* (*GOES-12*), Canadian Lightning Detection Network (CLDN) lightning, aircraft meteorological data relay (AMDAR) profiles, among others] were also utilized, as were data from the Weather Modification Inc. (WMI) C-band radar. The locations of EC's Strathmore (XSM) radar

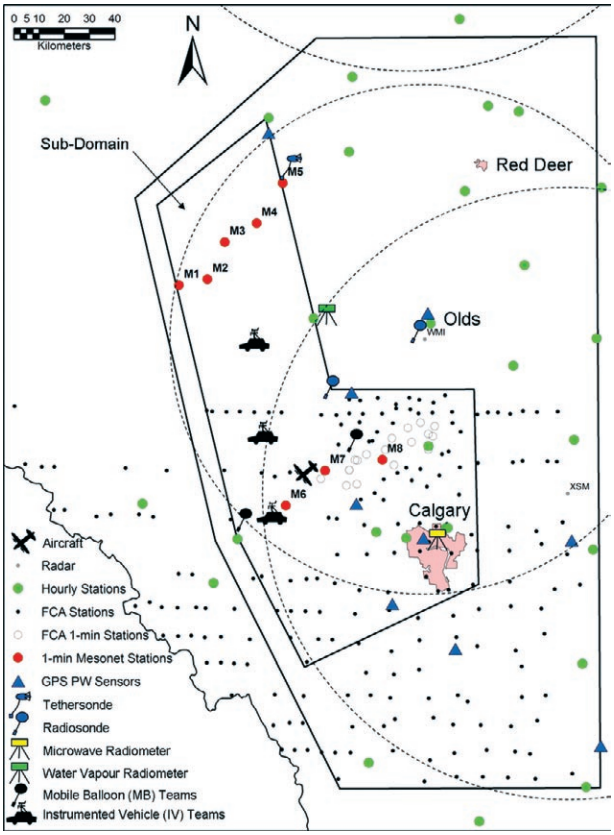


**Fig. 4. Instrumentation map for UNSTABLE 2008. Hourly surface stations (green circles) comprise the existing operational surface station network (black circles in Fig. 2). All other surface stations are unique to UNSTABLE 2008. Dashed circles are 120-km range rings (extent of Doppler coverage) for EC radars at Carvel and Strathmore and 100 km for the WMI radar near Olds (denoting the range for detection of 0-dBZ echoes). Actual aircraft, MB, and IV team positions varied from mission to mission.**

**Table 3. Special instrumentation deployed/utilized for UNSTABLE 2008; $T$ = temperature, $T_d$ = dewpoint temperature, RH = relative humidity, $p$ = station pressure, PCPN = liquid precipitation, RAD = total incoming solar radiation, Turb = turbulence, and VV = vertical velocity.**

| Instrument/network | Observation frequency | Parameters | Institution | Mobility | Operational period |
|---|---|---|---|---|---|
| **Surface observations**[a] | | | | | |
| 5 ATMOS[b] | 1 min | $T$, $T_d$, wind (10 m), $p$, PCPN, RAD, $\Delta T$ (9.5–0.5 m) | EC | Fixed | 15 Jun–15 Aug |
| 2 FOPEX | 1 min | $T$, $T_d$, $p$, PCPN, wind (2 m) | EC | Fixed | 9–23 Jul |
| 19 FCA | 1 min | $T$, $T_d$, PCPN | University of Calgary | Fixed | 9–23 Jul |
| 1 FCA | 1 min | $T$, $T_d$, wind (10 m), $p$, PCPN | University of Calgary | Fixed | 9–23 Jul |
| 215 FCA | 1 h | $T$, $T_d$, PCPN | University of Calgary | Fixed | 9–23 Jul |
| IV1 (AMMOS) | 2 s | $T$, $T_d$, wind (~3 m), $p$, lightning | EC | Mobile | 9–23 Jul [c] |
| IV2 | 15 s | $T$, $T_d$, $p$ | EC/G. S. Strong | Mobile | 9–23 Jul [c] |
| IV3 | 2 s | $T$, $T_d$, $p$ | EC | Mobile | 13–22 Jul [c] |
| WVX (radiosonde) | 1 min | $T$, $T_d$, wind (10 m), $p$ | EC | Fixed | 9–23 Jul |
| EA3 (radiosonde) | 10 min | $T$, $T_d$, wind (10 m), $p$ | WMI | Fixed | 9–23 Jul |
| MB1 | 1 min | $T$, $T_d$, wind (2 m), $p$ | EC | Mobile | 9–23 Jul [c] |
| MB2 (MARS) | 15 min | $T$, $T_d$, wind (~3 m), $p$ | University of Manitoba | Mobile | 9–23 Jul [c] |
| Hail pads | 2–5-km paths | Hail size distribution and impact energy density | G. S. Strong | Fixed | 8 Jul–29 Aug [c] |
| **Upper air/profiling** | | | | | |
| WVX radiosonde | 2 s | $T$, $T_d$, wind, $p$ | EC | Fixed | 9–23 Jul |
| EA3 radiosonde | 2 s | $T$, $T_d$, wind, $p$ | WMI | Fixed | 9–23 Jul |
| MB1 radiosonde | 2 s | $T$, $T_d$, wind, $p$ | EC | Mobile | 9–23 Jul [c] |
| MB2 radiosonde (MARS) | 2 s | $T$, $T_d$, wind, $p$ | EC/University of Manitoba | Mobile | 9–23 Jul [c] |
| AERI (MARS) | 15 min | Up to 3 km $T$, RH | University of Manitoba | Mobile | 9–23 Jul [c] |
| IR pyrometer (MARS) | 6 s | Cloud-base $T$ | University of Manitoba | Mobile | 9–23 Jul [c] |
| Doppler sodar | 15 min | Up to 1.3-km wind, VV, mixing depth, Turb. | University of Manitoba | Fixed | 9–23 Jul [c] |
| Tethersonde | 10 s | $T$, $T_d$, wind, $p$ | EC | Fixed | 9–23 Jul |
| Profiling microwave radiometer | 10 s | Up to 10-km RH, liquid $H_2O$, integrated water | University of Calgary | Fixed | 9–23 Jul |
| **Total column water vapor** | | | | | |
| 9 GPS PW sensors | 30 min | PW | University of Calgary | Fixed | 9–23 Jul |
| Water vapor radiometer | 10–30 s | Water vapor, liquid $H_2O$ | University of Calgary | Fixed | 9–23 Jul |
| Water vapor radiometer (MARS) | 45 s | Water vapor, liquid $H_2O$ | University of Manitoba | Mobile | 9–23 Jul [c] |
| **Aircraft** | | | | | |
| Aventech AIMMS-20[d] and Lyle Lilie microphysics | 1 s | $T$, $T_d$, $p$, microphysics | WMI | Mobile | 8–23 Jul [c] |

[a] IV observations were samples, whereas those from other stations were average values.

[b] ATMOS—Automated Transportable Meteorological Observation System.

[c] Instruments operating on IODs only (see Table 5).

[d] AIMMS-20—Aircraft-Integrated Meteorological Measurement System.

and the WMI radar are shown with range rings in Fig. 4, as is a range ring from the Carvel (WHK) radar located to the north of the UNSTABLE domain. Radar "fine lines" (i.e., thin lines of enhanced radar reflectivity) have played an important role in past CI field studies because they often indicate the presence

| Table 4. UNSTABLE 2008 IOD missions and objectives. | |
|---|---|
| **IOD mission** | **Objectives** |
| CI 1 (ABL water vapor*) | Characterize the evolution of ABL water vapor within areas favorable for CI and the development of thunderstorms in the absence of well-defined mesoscale convergence boundaries |
| CI 2 (mesoscale boundary) | Sample environments near mesoscale boundaries and within associated circulations with the potential to trigger CI |
| Dryline | Resolve and characterize the 4D dryline environment with and without associated CI and thunderstorm development |
| Water vapor gradient 1 (soil moisture) | Sample horizontal water vapor gradients associated with discontinuities in soil moisture from agrometeorological model forecasts and observed areas of recent precipitation |
| Water vapor gradient 2 (vegetation) | Sample horizontal water vapor gradients associated with contrasting areas of vegetation type, specifically forested versus cropped areas |

*ABL water vapor in association with mesoscale convergence boundaries is captured in mission CI 2 (mesoscale boundary).

of low-level convergence boundaries (Wilson and Schreiber 1986; Browning et al. 2007; Buban et al. 2007). However, the sensitivity of the WMI radar was too low to detect all but the largest fine-line targets, and although the EC radars often detect fine lines, their distance from the region of most-frequent CI precluded frequent fine-line observations of the dryline. Mobile Doppler radar support was not pursued for the pilot experiment because of resource limitations, but it is planned for the full-scale UNSTABLE project to provide more complete radar-based observations of boundaries over the region.

All observational data have been quality controlled using standard methods. Observations from mobile platforms often required the most effort. The authors can be contacted for details.

*Field logistics.* The UNSTABLE 2008 field program took place during the nine weeks from 15 June to 15 August. This period captures the peak climatological period of thunderstorm and severe weather activity in Alberta. An intensive observation period (IOP) ran from 9 to 23 July, when mobile teams were on standby to conduct observations. Each day during the IOP, rawinsonde data were obtained at 1200 UTC (UTC is local daylight saving time plus six hours.) from the two fixed locations near the towns of Olds (EA3) and Water Valley (WVX). If mobile operations were conducted [an intensive observation day (IOD)], then additional sondes were released simultaneously every two hours until 0000 UTC by all four sounding teams. Predefined missions were developed, including proposed routes for mobile teams given limited road networks along the foothills. Mobile teams were vectored into position and monitored by a field coordinator (FC) at the WMI radar site just south of Olds, Alberta. Where possible, IOD missions were conducted in the vicinity of mesonet station lines to maximize the quantity of fixed and mobile data targeting a specific event. The mission objectives are summarized in Table 4. Each morning during the IOP, the principal investigators determined if operations should be conducted, and if so, they selected an appropriate mission. Sounding teams were usually located on either side of boundaries in adjacent areas of interest with IV teams conducting surface transects between sounding locations or on adjacent roads. Aircraft flights followed stepped traverses and spirals between the mobile sounding teams or a racetrack pattern as dictated by the mission. More details on observation strategies are available in the UNSTABLE 2008 Pilot Experiment Operations Plan (Taylor et al. 2008a).

During the UNSTABLE 2008 IOP, eight IOD missions were conducted with an additional day of partial operations. Down days were used for equipment maintenance and testing, logistical and mission reviews, and media interviews. An operational summary is provided in Table 5.

*Forecast/nowcast support.* Forecasting and nowcasting for UNSTABLE 2008 was collaborative between the FC and the dedicated staff from EC's Prairie and Arctic Storm Prediction Centre (PASPC). Each evening the FC would brief field teams on the potential for operations for the next day. The following morning, PASPC staff would provide a forecast to the FC on the convective potential for the current day (day 1) as well as an outlook for the next day (day 2). These would include graphical depictions posted to an internal government

| Table 5. UNSTABLE 2008 operational summary and IOP highlights. | | |
|---|---|---|
| **Date** | **Mission/activities** | **Events/highlights** |
| 8 Jul | Media and testing | Media day with local TV, radio, and newspaper journalists; tests and measurement comparisons among mobile surface teams, radiosonde, and aircraft |
| 9 Jul | Dryline | Dryline development and interaction with multiple outflow boundaries; severe storms in northern region of UNSTABLE domain |
| 12 Jul | Water vapor gradient 1 | Attempted to resolve ABL moisture gradient due to soil moisture differences; actual soil moisture gradient likely resided outside UNSTABLE domain, hampering results |
| 13 Jul | Dryline | Dryline development and interaction with outflow boundaries; CI outside UNSTABLE domain; storm evolution and severe hail within domain |
| 14 Jul | Dryline | Low expectations for quasi-stationary dryline near Rocky Mountains; IV1 (AMMOS) sampled dryline west of UNSTABLE domain; subsidence in lee of mountains inhibited CI |
| 15 Jul | Partial operations—CI 2 (mesoscale boundary) | IV1 and MB2 teams attempted to capture CI at southern extent of UNSTABLE domain; storms that initiated in domain produced severe hail and a weak tornado, and later produced widespread wind damage south of UNSTABLE domain |
| 16 Jul | Damage survey—Vulcan–Medicine Hat area | UNSTABLE personnel participated in damage survey from storms on 15 Jul |
| 17 Jul | CI 1 (ABL water vapor) | Mesoscale boundary and CI within UNSTABLE domain; severe hail observed in domain |
| 20 Jul | Water vapor gradient 2 | Observations of ABL evolution over adjacent cropped and forested areas |
| 21 Jul | CI 2 (mesoscale boundary) | Sampling of multiple mesoscale boundaries in the UNSTABLE domain, warm-air aloft inhibited CI |
| 22 Jul | CI 1 (ABL water vapor) | Deck of stratocumulus/cumulus inhibited sufficient insolation over foothills and potential for mesoscale circulation |

Web page. The PASPC meteorologist would also construct graphical mesoanalyses each hour in support of field operations. The FC and the PASPC meteorologist frequently coordinated during the day's operations.

*High-resolution NWP model support.* The Canadian Meteorological Centre (CMC) has been running a convective-scale version of the GEM model over various domains in Canada since 2005. EC provided specialized NWP support for UNSTABLE 2008 in the form of limited-area model (LAM) runs of GEM at 2.5- and 1.0-km horizontal grid spacing. The 2.5-km run (GEM-LAM-2.5) was initialized using boundary conditions from the variable-resolution (15 km over Canada) global GEM model run that is used to provide short-term (48 h) NWP forecasts for the entire country. No additional data assimilation was performed for the 2.5- or 1-km grid. The domain covered most of the provinces of British Columbia and Alberta (Fig. 5) and was integrated out to 24 hours daily, starting at 1200 UTC. A special 1-km GEM-LAM grid (Fig. 5) was run every day in real time from 1500 to 0300 UTC for the 3-month period of 1 June–31 August 2008. The 1-km model (GEM-LAM-1) was nested within the GEM-LAM-2.5 west domain and initialized from its 3-h forecasts with horizontal boundary conditions supplied every 1 hour thereafter. The model configuration was similar to the GEM-LAM-2.5 but used a reduced time step, an increased frequency for calling the radiation scheme (every 15 minutes), and an experimental two-moment bulk microphysics scheme (Milbrandt and Yau 2005). Also, a special technique of gradually evolving the model orography from a resolution of 2.5 km (that of the driving model) to 1 km over a period of two hours was employed. This reduces the introduction of numerical instability caused by sudden increases or decreases in the height of the lowest model level (McTaggart-Cowan et al. 2010). Both the GEM-LAM-2.5 and the GEM-LAM-1 use terrain-following vertical coordinates with vertical spacing increasing with elevation, ranging from approximately 40 m near the surface to 200 m near 1.5 km above ground (typically ~10 model levels). Surface characteristics used in GEM-LAM-2.5 and GEM-LAM-1 are derived from a high-resolution (1 km or less horizontal resolution) database of 26 distinct land use/land surface types. Surface prognostic variables for a nested run are interpolated from the driving model; thus, for the 1-km run, these surface variables ultimately come

from the 15-km GEM forecasts since currently there are no independent analyses produced for the higher-resolution grids. Other aspects of the model configurations are summarized in Table 6.

A Web site was set up to display images of model output, from both the GEM-LAM-2.5 and the GEM-LAM-1, for use by UNSTABLE participants. Two sets of fields were produced, including a set of standard model fields plus a set of special convective diagnostic fields developed at EC's Hydrometeorology and Arctic Laboratory (see Table 7). The Web site allowed participants to view the model forecast fields and make direct comparisons between the behavior of the GEM-LAM on the 2.5- and 1-km grids. These real-time forecasts were routinely used for operational planning and mission decisions during the IOP.

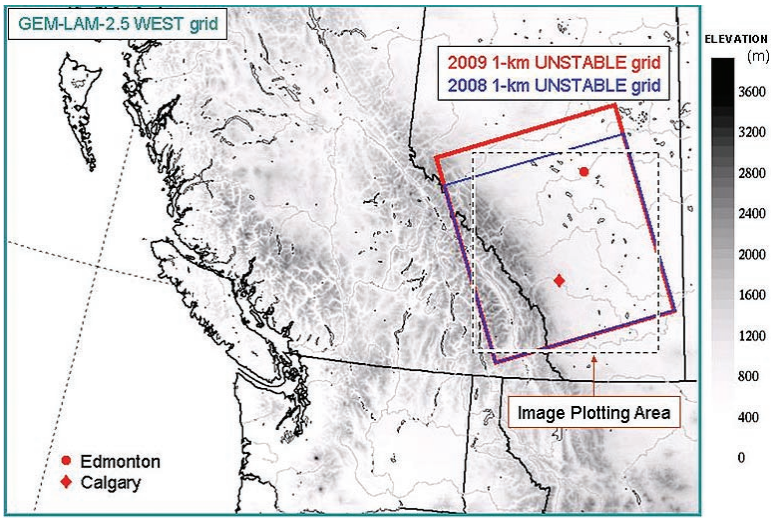


**Fig. 5. Domains of the 2.5- and 1-km GEM-LAM configurations used for real-time forecasts during UNSTABLE. Shading represents model topography. "Image plotting area" refers to the portion of the model domain used to produce Web-based forecast imagery in support of UNSTABLE 2008 operations.**

To pursue Q3 and to continue to work toward providing improved high-resolution NWP support for future UNSTABLE field work, the GEM-LAM-1 was run again during the summer of 2009. All model output and Web site images for the 2008 and 2009 summers are archived for examination related to the science questions and for other research purposes.

We remark that the NWP component of the experiment was somewhat distinct from the observational component (Q1 and Q2), in that its purpose was not to research CI directly. Given that operational forecasting today relies heavily on NWP guidance and that UNSTABLE provides a unique dataset, the inclusion of Q3 was a logical component of the project. Note that for the 2008 pilot campaign, no assimilation of the special observations into the 1-km (or 2.5 km) model was performed. At the time of the experiment, it was not possible to assimilate data onto a limited-area grid in the GEM. High-resolution data assimilation will be considered for the future full-scale experiment.

**PRELIMINARY RESULTS.** *Mesoscale boundaries.* One objective of UNSTABLE is to improve our

**Table 6. Configuration details and parameterizations for the GEM-LAM; *dx*, *dt*, PBL, TKE denote horizontal grid spacing, time step, planetary boundary layer, and turbulent kinetic energy, respectively.**

| Model detail | GEM-LAM-2.5 | GEM-LAM-1 |
|---|---|---|
| *dx* | 2.5 km | 1 km |
| *dt* | 60 s | 30 s |
| PBL scheme | TKE based (Benoit et al. 1989) | Same |
| Convective scheme | — | Same |
| Explicit condensation scheme | Single moment (Milbrandt and Yau 2005) | Double moment (Milbrandt and Yau 2005) |
| Land surface scheme | Bélair et al. 2003 | Same |
| Solar radiation scheme | Fouquart and Bonnel (1980) | Same |
| Infrared radiation scheme | Garand and Mailhot (1990) | Same |
| Horizontal diffusion | Explicit | Same |
| Vertical diffusion | Implicit | Same |
| Vertical coordinate | Hybrid pressure–Eta (unstaggered) | Charney–Phillips (staggered) |

**Table 7. Images computed from GEM-LAM-2.5 and GEM-LAM-1 model outputs, available to UNSTABLE participants via internal Web page; sfc denotes surface, LCL denotes lifting condensation level, MLLFC denotes mixed layer level of free convection, MLCAPE denotes mixed-layer CAPE, and SBCAPE denotes sfc-based CAPE. The list of convective diagnostics includes experimental fields under development at EC's Hydrometeorology and Arctic Lab.**

| Standard diagnostics | Convective diagnostics |
|---|---|
| Bowen ratio (sfc) | Bulk shear, sfc–1 km |
| Dewpoint temperature and winds (sfc) | Bulk shear, sfc–LFC |
| Divergence and winds (sfc) | CAPE, mixed layer based (0–3 km) |
| Latent heat flux (sfc) | CAPE, sfc based |
| Precipitation accumulation | CIN, mixed layer based |
| Precipitation rates | CIN, sfc based |
| Reflectivity, 1.5-km CAPPI | Depth of ABL convergence |
| Reflectivity, 7.0-km CAPPI | Depth of ABL well-mixed vapor |
| Reflectivity, column maximum | Dewpoint temperature, lowest 50 hPa |
| Sensible heat flux (sfc) | LCL height, mixed layer based |
| Specific humidity and winds (sfc) | LCL height, sfc based |
| Temperature and pressure (sfc) | LFC height, mixed layer based |
| Vertical motion and winds (near sfc) | LFC height, sfc based |
| Vorticity and winds (near sfc) | Mean wind, 0–6 km AGL |
| | Normalized CAPE |
| | Ratio of ABL convergence depth to MLLFC height |
| | Ratio of MLCAPE to SBCAPE |

understanding of how mesoscale boundaries and circulations promote CI (see Q1). On 13 July 2008, a dryline was detected within the UNSTABLE domain via multiple observation platforms. CI appears to have occurred along this boundary outside of the UNSTABLE domain, with subsequent storms producing severe hail (up to ~45 mm in diameter) within the UNSTABLE domain. This case is used to illustrate how UNSTABLE 2008 observations help to characterize mesoscale boundaries observed in this region.

A comparison of objective isodrosotherm analyses using

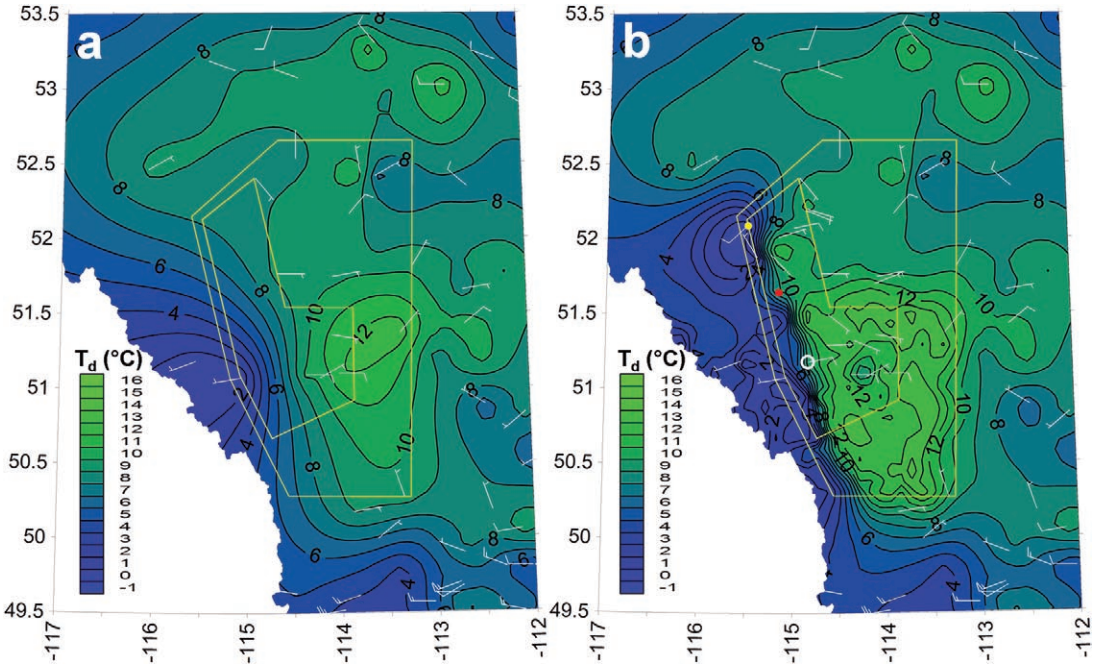


**Fig. 6. Objective surface isodrosotherm analysis for 2100 UTC 13 Jul 2008. (a) Observations from the existing real-time synoptic operational network. (b) Observations including the UNSTABLE 2008 network. Latitude and longitude (°) are indicated at left and bottom of maps. Position of IV1 (IV2) teams indicated by yellow (red) dot. Open white circle indicates the location of M6 (see text). Wind is in m $s^{-1}$ (1/2 barb = 2.5 m $s^{-1}$, full barb = 5 m $s^{-1}$).**

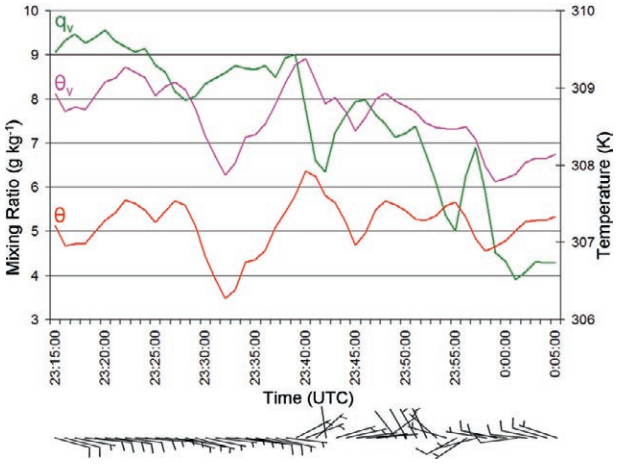


**Fig. 7. Dryline passage at M6 from 1-min-average data (see Fig. 4) from 2315 UTC 13 Jul 2008 to 0005 UTC 14 Jul 2008. Data are $q_v$ (g kg$^{-1}$), $\theta$ (K), virtual potential temperature $\theta_v$ (K), and wind (1/2 barb = 2.5 m s$^{-1}$, full barb = 5 m s$^{-1}$).**

the existing operational and UNSTABLE 2008 surface observation networks is shown in Fig. 6 for 2100 UTC 13 July 2008. Although the operational network resolves a weak gradient in dewpoint (and $q_v$, not shown), the UNSTABLE 2008 observations resolve the dryline via a much stronger gradient in dewpoint and $q_v$ (not shown). The additional wind observations in the UNSTABLE network suggest that an area of enhanced convergence may be collocated with the dryline. Existing real-time observations often provide little information on near-surface meteorological conditions over the foothills.

Surface observations were recorded as 1-min averages (fixed) and 2–15-s samples (mobile) to allow for detailed characterization of mesoscale features of interest. Passage of a dryline through station M6 (located 55 km west-northwest of Calgary) is illustrated via 1-min observations in Fig. 7. These observations highlight the detailed structure of the boundary, resolving multiple thermal and moisture gradients and wind shifts (convergence zones). The primary instrumented vehicle (IV1) used in UNSTABLE 2008 (see Table 3) recorded wind data in addition to thermodynamic parameters. The structure of the same dryline that passed M6 was resolved with 2-s data by IV1 (Fig. 8) more than 100 km northwest of station M6 (see Fig. 6b). While traveling northeast at an average speed of 14 m s$^{-1}$ (49 km h$^{-1}$), IV1 sampled multiple moisture gradients within the dryline over a distance of only 630 m. The overall gradient in dewpoint ($q_v$) was 13°C km$^{-1}$ (6 g kg$^{-1}$ km$^{-1}$) over 630 m, with embedded gradients as strong as 42°C km$^{-1}$ (18 g kg$^{-1}$ km$^{-1}$). Orientation of the boundary was from northwest to southeast; therefore, transitions from a southerly/westerly wind to a northerly/easterly wind indicate convergence. The return of wind direction to southerly on the moist side of the dryline may be due to local terrain effects and is a topic for further analysis. Data from transects conducted by IV2 (not shown) suggest that the horizontal position of the dryline oscillated over a distance of 6 km before the boundary advanced eastward after 2100 UTC. Dryline width and moisture gradients from IV2 data are comparable to those shown for IV1. A number of other narrow boundaries with sharp thermodynamic gradients (e.g., storm gust fronts, dryline–outflow merged boundaries) were sampled by the IVs during the IOP.

Aboveground observations during UNSTABLE were obtained mainly via strategically placed rawinsonde teams and instrumented aircraft. During UNSTABLE 2008, 2-hourly simultaneous soundings were obtained on either side of mesoscale boundaries whenever possible. Soundings valid at 0000 UTC on either side of the 13 July 2008 dryline are shown in Fig. 9. The "dry"

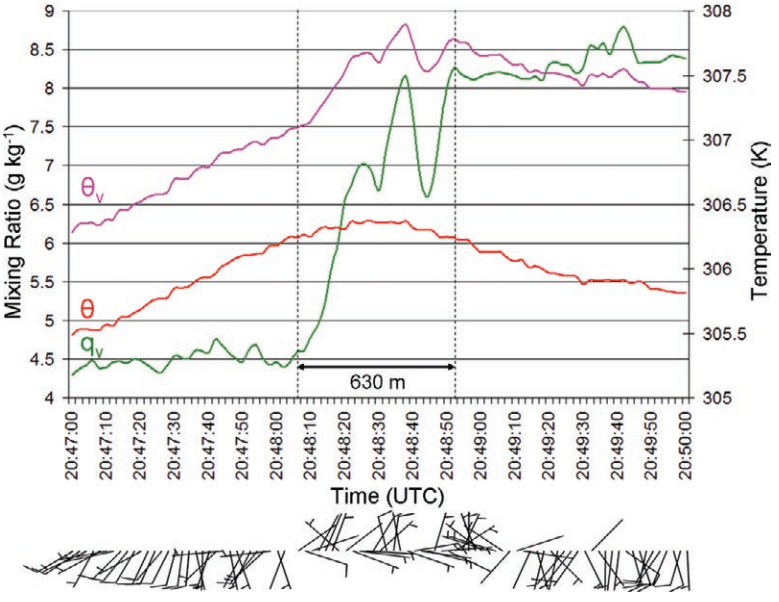


**Fig. 8. IV1 (AMMOS) sampling of a dryline from 2047 to 2050 UTC 13 Jul 2008. Observations collected were 2-s samples. The vehicle was traveling northeast at an average speed of 49 km h$^{-1}$ (14 m s$^{-1}$). Data are as in Fig. 7. The width of the boundary is 630 m, as determined using IV1 GPS position data.**

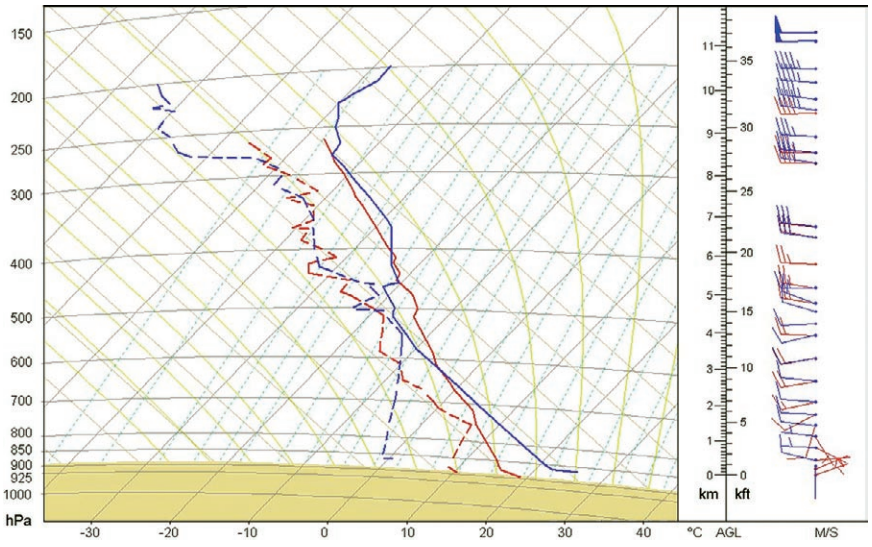


**Fig. 9. Tephigram showing mobile soundings valid 0000 UTC 14 Jul 2008 on the dry side (MB1, blue) and moist side (MB2, red) of the dryline. Temperature (dewpoint) curves are solid (dashed). Pressure data are in hPa, and wind data are in m s$^{-1}$ (1/2 barb = 2.5 m s$^{-1}$, full barb = 5 m s$^{-1}$).**

sounding (MB1) was within 10 km of the dryline and shows a deep, well-mixed ABL that is warmer and significantly drier than the "moist" MB2 sounding. The MB2 sounding was ~35 km from the boundary and is characterized by a shallower, cooler, and more moist ABL. Although an outflow boundary had passed through the location of MB2 shortly before the sounding, the surface $\theta$ analysis, including nearby sites (not shown), is consistent with the soundings showing a thermal gradient across the dryline. A more-detailed analysis of these soundings and a comparison to the existing dryline conceptual model were discussed in Taylor et al. (2008b). Soundings from this and other IODs are being analyzed to characterize ABL and upper-air conditions near boundaries and other features of interest.

Aircraft observations were obtained from 1755 to 1923 UTC in the vicinity of the dryline on 13 July 2008. Observations currently consist of thermodynamic variables only, as complications in the calibration of wind measurements remain unresolved at the time of writing. A combination of spiral and stepped traverse flight paths were used in an attempt to resolve characteristics of the boundary, and near boundary, ABL. The flight track from 13 July 2008, the surface observations at 1900 UTC, and the positions of mobile teams are illustrated in Fig. 10. The aircraft conducted seven traverses at altitudes ranging from a few hundred to 1,500 m above ground level (AGL) over lower terrain. From aircraft, sounding, and surface observations, vertical cross sections of various parameters were created. A $q_v$ cross section is shown in Fig. 11. In the moist air, $q_v$ is generally well mixed over the lowest 2 km at distances of less than 20 km from point A in Fig. 10. The dryline boundary is resolved in the vertical approximately 60 km from point A. Undulations in $q_v$, and in $\theta$ (not shown), are evident at the top of the moist ABL and may be indicative of gravity waves or remnant horizontal roll circulations propagating over the capped ABL on the moist side of the dryline. Similar features have been observed in the vicinity of the dryline in the United States (e.g., Buban et al. 2007).

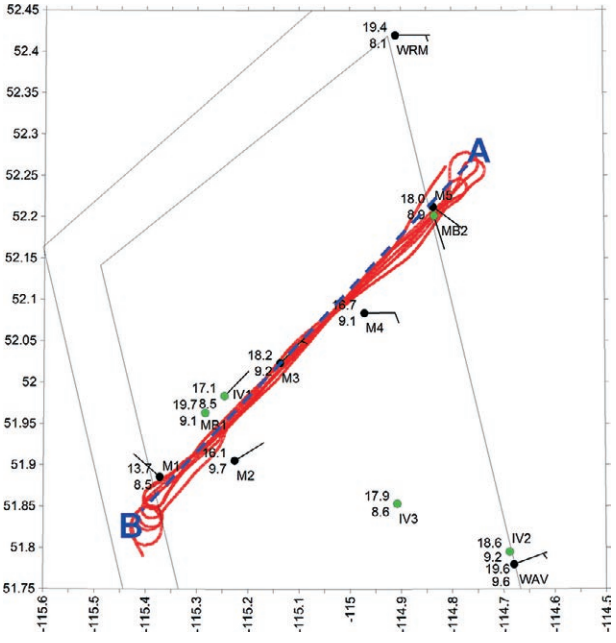


**Fig. 10. Aircraft flight track (red line) and surface observations [temperature (°C), dewpoint (°C), and wind (m s$^{-1}$) following standard surface plot conventions] at 1900 UTC 13 Jul 2008. Latitude and longitude (°) are indicated at left and bottom of maps. Green dots indicate mobile surface and radiosonde teams. Blue dashed line A–B indicates axis used for vertical cross section (see Fig. 11). Light-gray line indicates UNSTABLE domains. Wind data are in m s$^{-1}$ (1/2 barb = 2.5 m s$^{-1}$, full barb = 5 m s$^{-1}$).**

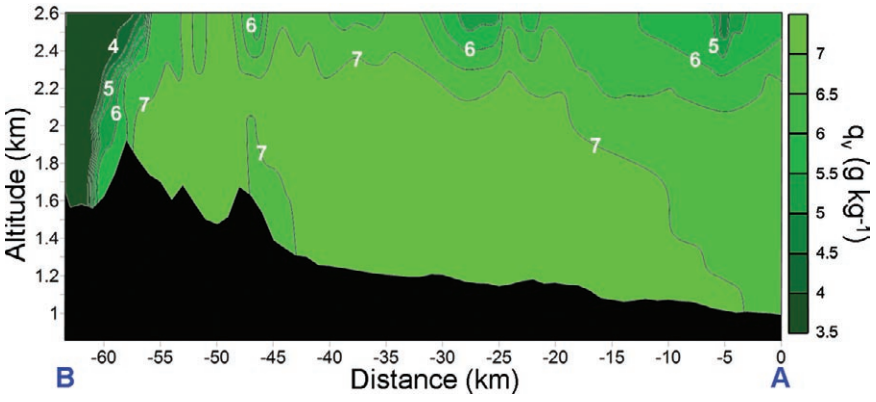


**Fig. 11. Vertical cross section of $q_v$ (g kg$^{-1}$) derived from aircraft (5-s average values from 1755 to 1923 UTC), radiosonde, and surface observations on 13 Jul 2008. Data were gridded to 500-m (100-m) resolution in the horizontal (vertical). Contours are every 0.5 g kg$^{-1}$ and labeled every 1 g kg$^{-1}$. Points A and B correspond to the positions indicated in Fig. 10. Horizontal distance is defined as the distance from point A to point B. Terrain is derived from U.S. Geological Survey digital elevation model (DEM) data along the path A–B and is exaggerated because of the expanded altitude scale.**

Preliminary results presented in this section illustrate one example of a mesoscale feature (i.e., a dryline) associated with CI in the Alberta foothills. Data from this and other IODs are revealing details about boundaries and CI mechanisms that have never been resolved in this region. These observations will allow for improved understanding of processes influencing CI in Alberta and help address issues considered under Q1. As these processes are better understood, they can be placed in context with CI mechanisms observed elsewhere. This will allow for refinement of existing conceptual models to be used by forecasters in conjunction with operational observation networks and NWP to improve forecasts of CI and severe storms.

*Surface effects on the ABL.* On 20 July 2008, a mission was conducted in support of Q2 to sample ABL character and evolution under weak-flow synoptic conditions to assess differences between the foothill boreal forest region and the cropped/grassland region to the east (Fig. 3). The forested region is characterized by coniferous trees with heights of ~15–30 m, whereas the cropped/grassland region is composed of cereal crops and prairie grassland. This was the first time that detailed measurements have been available for this purpose in this region of Canada. For this mission, MB2 [Mobile Atmospheric Research System (MARS)] was positioned at 52.04°N, 114.78°W in the cropped area, whereas MB1 was located at 51.93°N, 114.93°W in the forested area; both teams were in the field from 1500 to 2300 UTC (Fig. 12). Soundings valid at 1600, 1800, 2000, and 2200 UTC were obtained by both teams. Two IV teams (IV1 and IV2) conducted surface transects between the MB teams from 1600 to 2200 UTC (blue lines in Fig. 12). All teams were on narrow gravel roads; therefore, surface observations in the cropped area may be considered to be above the vegetation canopy, whereas observations in the forested region are within or below the tree canopy. The aircraft flew a racetrack pattern at six levels between 150 and 1,100 m AGL (red lines in Fig. 12) and was in flight from 1800 to 2030 UTC.

Hourly mesonet contour maps show temporal and spatial variations in surface $\theta$ and $q_v$ during the

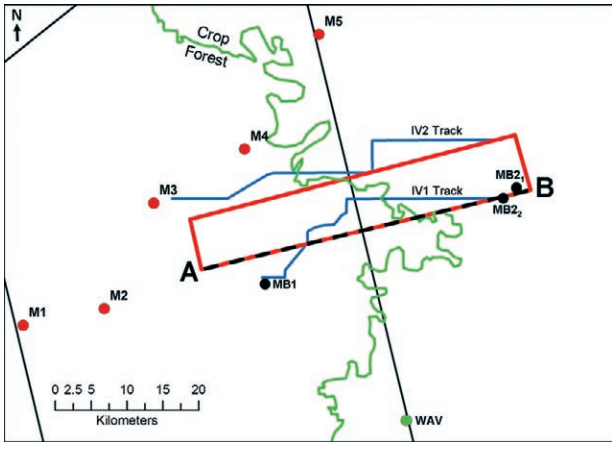


**Fig. 12. Instrumentation deployed for 20 Jul 2008. The green line is the approximate boundary between forested (west) and cropped (east) areas, as determined using satellite imagery and field observations. Locations are indicated for fixed mesonet stations (red circles), existing surface stations (green circles), and MB teams (black circles). The subscript 1 and 2 on MB2 indicates the early and later position of MB2, respectively, as the team had to relocate between 1800 and 2000 UTC soundings. Blue lines indicate predefined IV transects (actual IV1 observations extended slightly farther west and east). The aircraft flight path is indicated by the red box, and the black dashed line labeled A–B indicates the axis used to generate vertical cross sections (Fig. 14) and the graph in Fig. 15.**

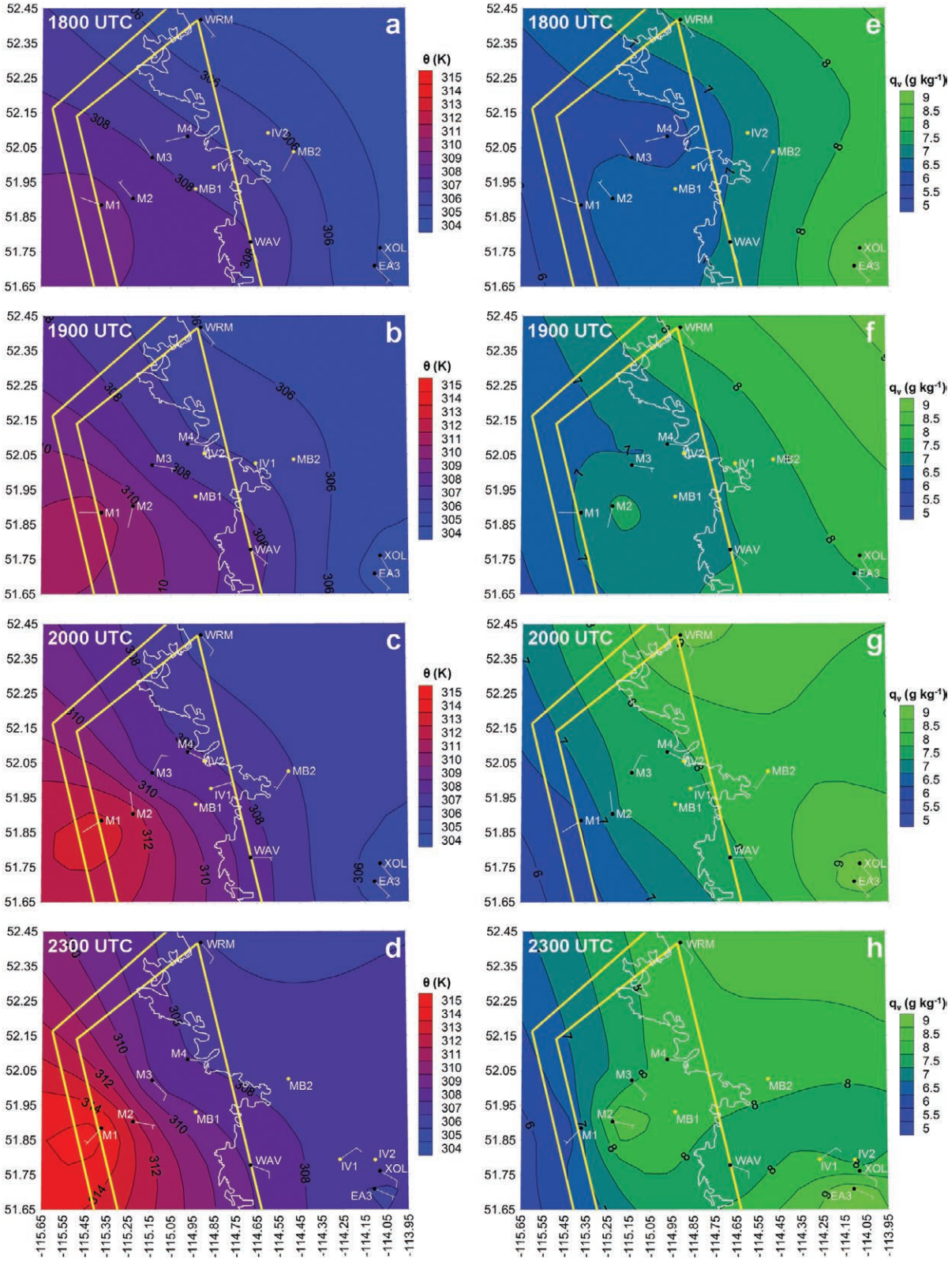


**FIG. 13. Mesonet contoured maps of (left) $\theta$ (K) and (right) $q_v$ (g kg$^{-1}$) from 20 Jul 2008 at (a),(e) 1800, (b),(f) 1900, (c),(g) 2000, and (d),(h) 2300 UTC. Latitude and longitude (°) are indicated at left and bottom of maps. Black dots are for fixed stations; yellow dots are for mobile stations. Wind data are in m s$^{-1}$ (1/2 barb = 2.5 m s$^{-1}$, full barb = 5 m s$^{-1}$). Yellow lines indicate the UNSTABLE domains. Light-gray line indicates the approximate location of the crop–forest boundary (as in Fig. 12).**

IOD (Fig. 13). Mesonet stations M1–M4 were within the forested region (M1 was farthest into the forest), with their locations progressively closer to the cropped area (see Figs. 12 and 13). Forest–crop differences in $\theta$ were 3–4 K between 1500 and 2000 UTC, and then they increased to 4–5 K between 2100 and 2300 UTC. The cropped region remained cooler than the forested area during the entire IOD (Figs. 13a–d). This was likely due to greater sensible heating (i.e., lower albedo and less ET) over the forested area, although no direct measurements were available to confirm this conclusion. The maps show the importance of mesonet data; the sharpest gradients occur where the spacing of stations is smallest. Gradients in $q_v$ were also captured by the mesonet with slightly higher $q_v$ in the cropped region (~7.5–8.5 g kg$^{-1}$) than in the western-most forested region (6.5–7.0 g kg$^{-1}$) during most of the IOD (Figs. 13e–h). Higher $q_v$ values persisted farther into the cropped areas throughout the entire IOD (not shown). By 2200 UTC, the $q_v$ gradient between station M1 (the station deepest into the forest) and the other stations strengthened. For example, Fig. 13h shows that $q_v$ at 2300 UTC increased to more than 8.0 g kg$^{-1}$ at M2 and M4, whereas M1 remained near 7.0 g kg$^{-1}$. Wind speeds were ~3 m s$^{-1}$ (10 km h$^{-1}$) or less most of the day over the entire domain, but then they increased to ~6 m s$^{-1}$ (20 km h$^{-1}$) from the southeast over much of the adjacent cropped region and into the forested area by 2200 UTC. It is likely that the wind advected moisture from the cropped region into portions of the forested region.

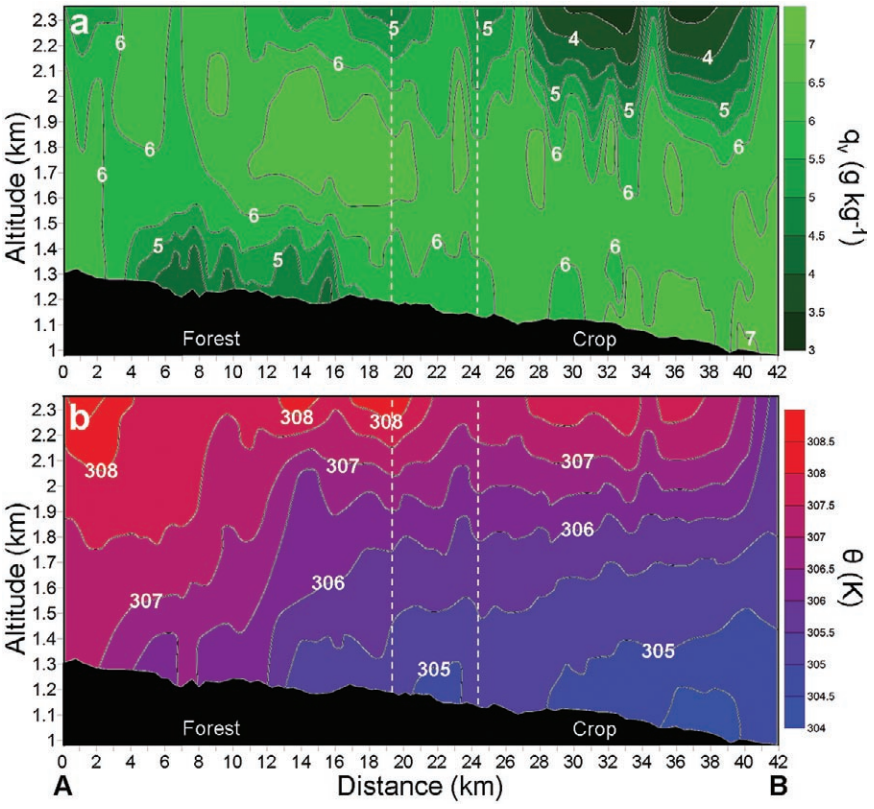


**Fig. 14. Vertical cross section of (a) $q_v$ (g kg$^{-1}$) and (b) $\theta$ (K) derived from aircraft (5-s average values from 1812 to 2029 UTC), radiosonde, and surface observations on 20 Jul 2008. Aircraft data are between points A and B in Fig. 12 and were gridded to 500-m (100-m) resolution in the horizontal (vertical). Horizontal distance is defined as the distance from point A to point B. Vertical dashed lines indicate a vegetation transition zone between the forest and crop areas at distances between ~19 and ~24 km. Terrain is derived from U.S. Geological Survey DEM data along the path A–B and is exaggerated because of the expanded altitude scale.**

Aircraft, IV1, and sounding data from MB1 and MB2 all depicted more distinct differences between the forested and cropped regions compared to the mesonet. Reasons for this may be due to contour interpolation and wider spacing of data points in the mesonet data. A vertical cross section derived from aircraft, sounding, and surface data (Fig. 14a) shows a clear gradient in $q_v$ of ~2.0–2.5 g kg$^{-1}$ at low levels between the 15-km point in Fig. 14a (forest) and the 35-km point (crops). The forested area shows a dry pocket ($q_v$ minimum of 4.5 g kg$^{-1}$) below 400 m AGL, whereas the cropped area has a maximum $q_v$ on the order of 7.0 g kg$^{-1}$. The moisture differences between cropped and forested regions are not apparent above 400 m AGL, mostly due to the aircraft being in the mid–upper portion of the ABL, as indicated by sounding analysis (see Fig. 16). Vertical profiles of $\theta$ from the soundings (Fig. 16) and Fig. 14b suggest that the cropped ABL depth was between 800 and 1,000 m AGL, whereas the forested ABL was deeper than this (almost 1,200 m) over the course of the flight. It should be emphasized that there was only one aircraft flight on this day to examine the spatial thermodynamic differences across the forest–crop

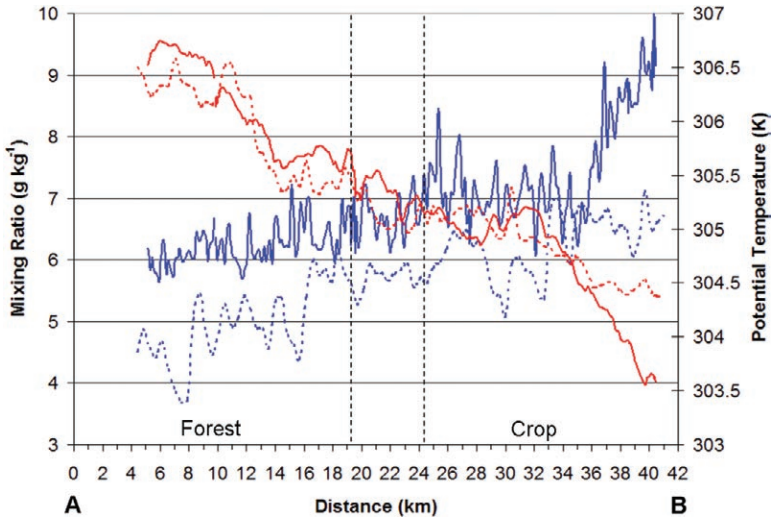


**Fig. 15. Plot of $\theta$ (red) and $q_v$ (blue) from the 1618 to 1721 UTC IV1 transect (solid) and lowest-level (150 m AGL) aircraft leg from 1802 to 1819 UTC (dashed) on 20 Jul 2008. Aircraft data are 5-s average values, and IV1 data are 10-s average values. Vertical dashed lines indicate a vegetation transition zone between the forest and crop areas at distances between ~19 and ~24 km. Points A and B are as in Fig. 12.**

boundary. We, therefore, do not know how these observations may have changed over the course of the day or even during the flight for any particular point in space. Two or more aircraft flights will be necessary for future missions.

Plots of $q_v$ and $\theta$ from an IV1 transect (1618–1721 UTC) are shown in Fig. 15 closest in time to the lowest-level (150 m AGL), southern-most aircraft pass (1802–1819 UTC). Both IV1 and aircraft data show similar spatial trends in $q_v$ and $\theta$ between the forested and cropped areas. The IV1 (aircraft) mixing ratios were 6.0–7.0 g kg$^{-1}$ (4.5–5.0 g kg$^{-1}$) in the forested region, 6.0–8.0 g kg$^{-1}$ (5.0–6.0 g kg$^{-1}$) in the western cropped areas, and up to 8.0–9.0 g kg$^{-1}$ (6.0–7.0 g kg$^{-1}$) farther into the crop region.

Comparisons of MB1 and MB2 sounding data reveal temporal thermodynamic variations in the vertical between the forested and cropped areas (Fig. 16). At 1600 UTC the lower ABL over the cropped region was capped and moist in comparison to the drier, well-mixed ABL over the forested region (Fig. 16a). By 1800 UTC the cap eroded and the cropped ABL became more well mixed but remained slightly more moist (by ~1 g kg$^{-1}$) and cooler (by ~2 K) than the forested region (Fig. 16b). Higher sensible heat fluxes over forested regions promote rapid development of a convective ABL and may lead to CI earlier than over cropped regions. Early-day development of a well-mixed ABL has been observed in previous Alberta field projects (e.g., LIMEX) and may distinguish ABL evolution in this region from other regions on the Canadian prairies. There was little difference in the vertical distribution of moisture between the two regions by 2000 UTC (except for the upper ABL discussed below); however, the forested region was still warmer than the cropped region by ~2 K (Fig. 16c). The ABL was consistently deeper over the forested region up to and including 2000 UTC, but the cropped ABL progressively deepened over the day.

Soundings at 1800 and 2000 UTC over the cropped area (MB2) show drying in the upper 100–200 m of the ABL (with ABL depth determined by rapidly increasing $\theta$ with height), whereas the MB1 soundings over the forested region do not (see Figs. 16b,c). The dry air in the upper ABL was most pronounced in the 1800 UTC profile (Fig. 16b). It is not known why this drying was present at some times and not others. However, various ABL phenomena may be responsible (e.g., bores, gravity waves, and small-scale turbulence).

The 20 July IOD in support of Q2 provided the first opportunity to examine the thermodynamic differences between forested and cropped regions in Alberta under weak synoptic-scale forcing conditions. This is important for better understanding the differences in ABL evolution between these two regions and how it may influence CI. Observations obtained across the forest–crop boundary (i.e., ABL height and thermodynamic evolution) provide insight into the partitioning of energy into sensible and latent heating over these areas in the absence of direct surface flux measurements. Under quiescent atmospheric conditions, the daily contribution of ET to moisture in the convective ABL, primarily through transpiration from vegetation, can exceed that added through advection (Raddatz 2005). Prairie boreal forests typically transpire between 2 and 3 mm day$^{-1}$ (Amiro et al. 2006; Barker et al. 2009) compared to wheat crops, which can transpire from less than 1 (water stressed) to more than 7 mm day$^{-1}$ (very little to no water stress) during the peak senescence period (Raddatz 2005; Brimelow et al. 2010). Vegetation (crops and perennial grasses) over most of central and southern Alberta did not experience moisture

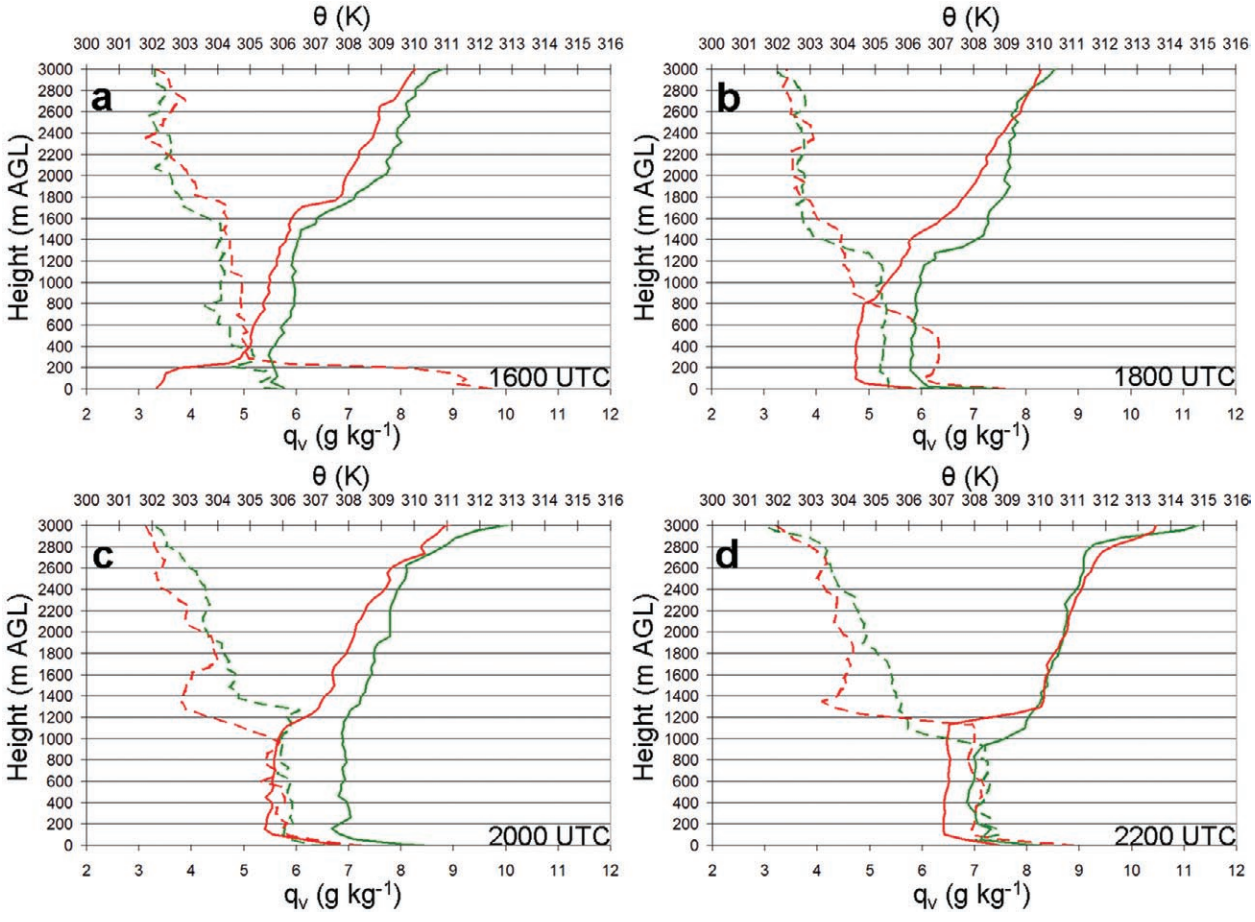


**Fig. 16. Four-panel graph of $\theta$ (solid) and $q_v$ (dash) from MB1 (green, forest land cover) and MB2 (red, crop land cover) soundings at (a) 1600, (b) 1800, (c) 2000, and (d) 2200 UTC 20 Jul 2008. Only the lowest 3,000 m AGL is shown.**

stress in July 2007, as suggested by the Canadian drought monitoring network (www.agr.gc.ca/pfra/drought/mapscc_e.htm) (not shown). Hence, local transpiration from these vegetation types was most likely normal to above average. The differences in evolution of ABL moisture and depth between the forested and cropped areas observed here suggest that the cropped/grassland region was likely transpiring to a greater degree than the forested region. This can have important consequences on days when deep convection is possible and when the mountain–plains circulation develops (Smith and Yau 1993a,b). Local ET appears to be an important source of ABL moisture, especially in central Alberta, where low-level moisture advection (without an ET contribution) can sometimes be extremely limited.

*High-resolution NWP.* In initial consideration of Q3, selected runs of the GEM-LAM at 1.0- and 2.5-km horizontal grid spacing were compared to observed radar. The GEM-LAM-1 frequently produced spurious, isolated convection during the summer of 2008 on days with even relatively mild convective instability, while the 2.5-km model was much less prone to this behavior. For example, Figs. 17a–c show simulated reflectivity at 1.5 km AGL for the GEM-LAM-2.5 and GEM-LAM-1 along with the observed radar 1.5-km constant altitude plan position indicator (CAPPI) valid at 1900 UTC 26 July 2008. Small convective cells were observed south of the Calgary region (approximately 120 km south of the Strathmore radar) and along the Rockies (just northwest of the project area). Although the GEM-LAM-2.5 captured the qualitative nature of the spotty convection, the GEM-LAM-1 produced spurious small-scale convection over a widespread region. This behavior occurred frequently throughout the summer of 2008 and, unfortunately, reduced the usefulness of the GEM-LAM-1 as a source of guidance for forecasting CI during the IOP.

In preparation for a later UNSTABLE experiment, the GEM-LAM-1 was modified and run again during

the summer of 2009 (on a slightly larger grid; see Fig. 5). To address the tendency to produce spurious convection in 2008, and based on experiences preparing for the 2010 Vancouver Olympics (Mailhot et al. 2010), the version of the dynamical core of the GEM model was updated to use a staggered (Charney–Phillips) vertical coordinate. For reasons that are hypothesized to pertain to improved temperature advection near the surface in sloped terrain, the 2009 configuration was essentially free of the problem of spurious convection for the GEM-LAM-1.

In general, the 1-km model did not improve the prediction of CI on 6 July 2008. In Figs. 17d–f, valid at 0100 UTC 6 July 2008, the occurrence of isolated cells south of the Carvel radar was more or less well simulated in both models (though with more convection in the GEM-LAM-1 compared to the GEM-LAM-2.5), whereas the convection predicted by both models east of the Strathmore radar is spurious. The fact that the spurious convection in the GEM-LAM-2.5 also occurs in the GEM-LAM-1 is not surprising since the GEM-LAM-1 is essentially a downscaling model, directly driven from the GEM-LAM-2.5 with no additional data assimilation. This illustrates that without improved initial conditions, the higher model resolution does not necessarily improve the numerical forecasting of CI.

For situations in which the numerical forecast of convection is reasonably good in the GEM-LAM-2.5, the GEM-LAM-1 often simulated a more realistic convective mode. For example, in Figs. 17g–i, valid at 0000 UTC 7 July 2008, although several individual model storms were spurious, the overall timing and location of convection in the GEM-LAM-2.5 was in reasonable agreement with the radar observations. However, the linear nature of the convective system near the Strathmore radar was better simulated by the GEM-LAM-1. In practice, the GEM-LAM-1 simulations may at times provide useful information on the convective mode and the type of severe weather elements that are expected.

Overall, we must conclude that without a high-resolution analysis to improve the initial conditions of the model, there is little evidence from the 2008 experiment that a single deterministic 1-km model will improve the forecast of CI over a 2.5-km configuration. Even with the improvements for the 2009 runs, the GEM-LAM-1 is driven by the GEM-LAM-2.5 and will therefore suffer from the same lack of mesoscale information in the initial data. It will be necessary to explore alternatives for high-resolution NWP guidance rather than simply using a 1-km downscaling model. Additional GEM-LAM results are being used to help address all three science questions in other ongoing, and future, studies.

**SUMMARY AND FUTURE RESEARCH.** Many observations from UNSTABLE 2008 are of spatial and temporal resolutions never before collected over the Alberta foothills and significantly exceed those of operational observation networks. During the 15-day IOP, eight IOD missions were conducted, including at least one of each predefined mission. A variety of fixed and mobile surface and upper-air instrumentation platforms were utilized to target observations characterizing mesoscale boundaries and ABL processes important for CI and severe storms in this region. High-resolution NWP output supported field operations and will be used for continued research in conjunction with field observations.

A variety of mesoscale boundaries were resolved in detail via UNSTABLE 2008 observations, including the most complete observations to date of a dryline in Canada. Significant moisture gradients (e.g., 18 g kg$^{-1}$ km$^{-1}$ in $q_v$) and wind convergence were observed over distances of less than 700 m. Even stronger gradients over shorter distances were recorded in other cases not reported here. Additional surface and upper-air observations characterize the 3D structure of the dryline. Future work will include NWP investigations of Alberta drylines, comparisons to dryline observations in the United States, and investigations of climatological dryline occurrence in Canada. In future field campaigns, we will endeavor to obtain more complete documentation of mesoscale boundaries and CI via additional targeted surface, radar, and aircraft observations. Understanding the development and behavior of the dryline and other mesoscale boundaries is critical for forecasters to anticipate how these features influence the timing and location of CI and to apply appropriate conceptual models when forecasting or nowcasting their occurrence, evolution, and potential interaction with local storms.

The evolution of the ABL over contrasting forested and cropped areas was investigated in detail for the first time in Alberta via meteorological measurements. From late morning through early afternoon, the ABL over the cropped area remained cooler, more moist, and shallower than the ABL over the forest. ET from crops may be an important local source of ABL moisture over the Alberta foothills, given the mountain barrier to the west and absence of significant nearby surface water sources (e.g., the Gulf of Mexico, the Great Lakes). Additionally, the interface between forested and cropped areas may be important for the development of local mesoscale boundaries/

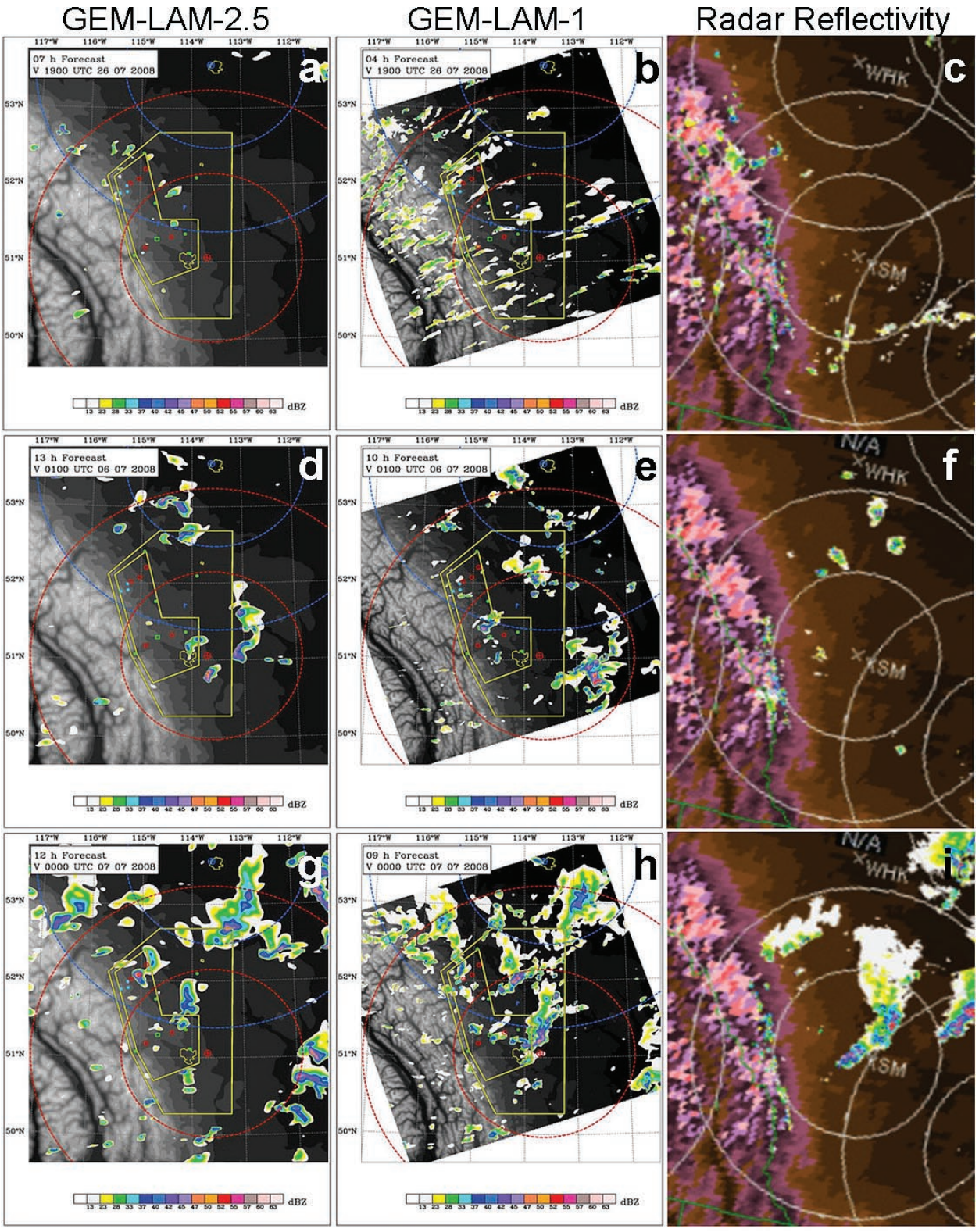


**Fig. 17. Synthetic model reflectivity from the (a),(d),(g) GEM-LAM-2.5 and (b),(e),(h) GEM-LAM-1 at 750 hPa (approximately equivalent to a 1.5-km AGL CAPPI) and (c),(f),(i) observed 1.5-km AGL CAPPI radar reflectivity at (a)–(c) 1900 UTC 26 Jul, (d)–(f) 0100 UTC 6 Jul, and (g)–(i) 0000 UTC 7 Jul 2008. Shown are 120- and 240-km range rings for the Carvel (blue) and Strathmore (red) radars. Model and observed radar plots use the same color scale for reflectivity. Gray shading for the (a),(d),(g) and (b),(e),(h) plots denotes model orography; brown shading in (c),(f),(i) denotes actual elevation.**

circulations that may influence the timing and location of CI. Detailed analysis of this case is ongoing with respect to a more quantitative comparison between soundings, analysis of tethersonde data, examination of the spatial and temporal variations of the IV data, and comparisons of all observational data to simulations from the GEM-LAM-1 and GEM-LAM-2.5. Of particular interest is the representation of modeled surface fluxes and the associated moisture field and ABL evolution. Future field work will include aircraft flux measurements over various vegetation and terrain features to better quantify spatial latent and sensible heat fluxes, vertical motion, and surface skin temperatures explicitly, similar to other field projects (e.g., Lemone et al. 2007).

High-resolution NWP model runs supported UNSTABLE 2008 operationally, and they form a significant component of ongoing and future research. Daily runs from 2009, when contrasted with those from 2008, highlighted improvements made to reduce a known problem with spurious convection. Output from the 2.5- and 1-km GEM-LAM configurations during the field campaign suggests that there may be limited benefit to simply downscaling to 1-km horizontal grid spacing without assimilation of additional data. The technology is now in place to perform high-resolution data assimilation in the GEM on a limited-area grid, and researchers at EC are currently working to produce 2.5-km analyses to initialize the GEM-LAM-2.5 (Fillion et al. 2010). Although there may be some utility in terms of forecasting convective mode with a single deterministic 1-km grid, the large uncertainties associated with high-impact weather indicate that a probabilistic approach is likely necessary for convective-scale forecasting (Stensrud et al. 2009). The use of an ensemble of slightly coarser-resolution convection-permitting grids (such as 2.5 km) will be explored in preparation for the full UNSTABLE experiment. Output from GEM-LAM-2.5 and GEM-LAM-1 will play an important role in continued analysis of UNSTABLE cases in support of each of the three main science questions.

UNSTABLE 2008 field operations provided an opportunity to test measurement strategies that may be considered for a larger-scale experiment. Tentative plans are to undertake another UNSTABLE field campaign in 2013, contingent on funding availability and other factors. Preliminary results have indicated a number of requirements for a future field campaign, including the following:

- Aircraft instrumented for eddy-correlation surface flux measurements and 3D winds
- Additional Automated Mobile Meteorological Observation System (AMMOS)-type IVs with wind measurement capability
- Mobile Doppler radar, and fixed radar with refractivity capabilities, to detect low-level features in active CI areas (e.g., radar fine lines, high-resolution horizontal moisture distribution) that are beyond the range and capability of existing operational radars; mobile Doppler radar may allow for dual-Doppler wind retrievals when the mobile Doppler lobe overlaps that of an existing Doppler radar
- Additional fixed mesonet stations in a grid configuration to complement the two mesonet station lines installed in 2008; some stations are required closer to the Rocky Mountains to better capture the development phase of the dryline, ABL evolution, and other features
- Additional profiling radiometers and sonic wind profilers to monitor ABL evolution with respect to thermodynamics and wind
- A number of fixed eddy-correlation flux systems situated over land cover areas of interest, for example, adjacent crop and forest regions
- A network of soil moisture measurements
- A longer IOP, increasing the likelihood of capturing multiple features or events of interest
- An ensemble high-resolution NWP system

The overall goal of UNSTABLE is to help forecasters issue the most timely and accurate severe thunderstorm watches and warnings possible. As detailed analysis of UNSTABLE data continues, and our understanding of CI processes in Alberta (and elsewhere) grows, researchers will endeavor to work with forecasters to utilize results in an operational setting. This will allow forecasters to better anticipate CI and severe weather, recognize limitations of real-time observations, and apply appropriate conceptual models when making watch/warning decisions in high-impact weather situations.

**ACKNOWLEDGMENTS.** The UNSTABLE 2008 field campaign was largely funded by Environment Canada (EC), but it relied extensively on in-kind and other support from a large number of individuals. The authors wish to thank EC managers Stewart Cober, Gary Burke, Bob Kochtubajda, Brian Wiens, Anne Walker, and Carol Klaponski for helping to champion UNSTABLE and to secure funding and other resources. Financial and infrastructure support to J. M. Hanesiak was provided by the Canada Foundation for Innovation (CFI); Natural Sciences and Engineering Research Council (NSERC); the

Drought Research Initiative (DRI) Network, supported by the Canadian Foundation for Climate and Atmospheric Sciences (CFCAS); and the Clayton H. Riddell Faculty of Environment, Earth, and Resources at the University of Manitoba.

We would also like to acknowledge data provision, instrumentation leads, and technical support from Shawn Marshall (University of Calgary), Gerhard Reuter (University of Alberta), Terry Krauss (Weather Modification Inc.), Pat King, Andrew Sheppard, Ron Goodson, Dave Patrick, Jeff Sowiak, William Burrows, Andrew Giles, Emma Hung, Steve Brady, Ron McTaggart-Cowan, and Blaine Lowry (all from EC). Forecast and nowcast support was provided by dedicated forecasters Steve Knott, Chris Wielki, and Dave Carlsen from EC's Prairie and Arctic Storm Prediction Centre (PASPC).

The authors would like to thank explicitly all the other field participants, whose dedication, expertise, and many hours in the field were critical for the success of the field campaign, including Andrew Giles, William Burrows, Shannon Moodie, Jay Anderson, Bruce Cole, Danny Brown, Erin Thompson, Joe Misfeldt, Garry Toth, Dave Carlsen, Paul Sirvatka, Jason Goehring, Viktor Makitov, Zac Glass, Bob Gorman, Joe Wiley, Jeff Allen, Manda Adams, Rhiannon Davies, Mark Firmin, Lesley Elliott, and Marshall Elliott.

Comments from two anonymous reviewers significantly improved the final manuscript.

## REFERENCES

Amiro, B. D., and Coauthors, 2006: Carbon, energy and water fluxes at mature and disturbed forest sites, Saskatchewan, Canada. *Agric. For. Meteor.,* **136,** 237–251.

Barker, C. A., B. D. Amiro, H. Kwon, B. E. Ewers, and J. L. Angstmann, 2009: Evapotranspiration in intermediate-aged and mature fens and upland black spruce boreal forests. *Ecohydrology,* **2,** 462–471.

Bélair, S., L.-P. Crevier, J. Mailhot, B. Bilodeau, and Y. Delage, 2003: Operational implementation of the ISBA land surface scheme in the Canadian regional weather forecast model. Part I: Warm season results. *J. Hydrometeor.,* **4,** 352–370.

Benoit, R., J. Côté, and J. Mailhot, 1989: Inclusion of a TKE boundary layer parameterization in the Canadian regional finite-element model. *Mon. Wea. Rev.,* **117,** 1726–1750.

Brimelow, J. C., J. M. Hanesiak, R. L. Raddatz, and M. Hayashi, 2010: Validation of ET estimates from the Canadian prairie agrometeorological model for contrasting vegetation types and growing seasons. *Can. Water Res. J.,* **35,** 209–230.

Browning, K. A., and Coauthors, 2007: The Convective Storm Initiation Project. *Bull. Amer. Meteor. Soc.,* **88,** 1939–1955.

Buban, M. S., C. L. Ziegler, E. N. Rasmussen, and Y. P. Richardson, 2007: The dryline on 22 May 2002 during IHOP: Ground-radar and in situ data analyses of the dryline and boundary layer evolution. *Mon. Wea. Rev.,* **135,** 2473–2505.

Bunkers, M. J., B. A. Klimowski, and J. W. Zeitler, 2002: The importance of parcel choice and the measure of vertical wind shear in evaluating the convective environment. Preprints, *21st Conf. on Severe Local Storms,* San Antonio, TX, Amer. Meteor. Soc., P8.2.

Chisholm, A. J., 1973: Part I: Radar case studies and airflow models. *Alberta Hailstorms, Meteor. Monogr.,* No. 36, Amer. Meteor. Soc., 1–36.

——, and J. H. Renick, 1972: The kinematics of multicell and supercell Alberta hailstorms. Alberta hail studies: 1972, Alberta Research Council Hail Studies Rep. 72-2, 24–31.

Craven, J. P., R. E. Jewell, and H. E. Brooks, 2002: Comparison between observed convective cloud-base heights and lifting condensation level for two different lifted parcels. *Wea. Forecasting,* **17,** 885–890.

Côté, J., S. Gravel, A. Méthot, A. Patoine, M. Roch, and A. Staniforth, 1998: The operational CMC–MRB Global Environmental Multiscale (GEM) model. Part I: Design considerations and formulation. *Mon. Wea. Rev.,* **126,** 1373–1395.

Crook, N. A., 1996: Sensitivity of moist convection forced by boundary layer processes to low-level thermodynamic fields. *Mon. Wea. Rev.,* **124,** 1767–1785.

Damiani, R., B. Geerts, J. Demko, S. Haimov, J. French, J. Zehnder, A. Razdan, J. Hu, J. Petti, M. Leuthold, G. S. Poulos, 2008: The Cumulus, Photogrammetric, In Situ, and Doppler Observations Experiment of 2006. *Bull. Amer. Meteor. Soc.,* **89,** 57–73.

Doran, J. C., W. J. Shaw, and J. M. Hubbe, 1995: Boundary layer characteristics over areas of inhomogeneous surface fluxes. *J. Appl. Meteor.,* **34,** 559–571.

English, M., 1973: Part II: Growth of large hail in the storm. *Alberta Hailstorms, Meteor. Monogr.,* No. 36, Amer. Meteor. Soc., 37–98.

Entekhabi, D., I. Rodriguez-Iturbe, and F. Castelli, 1996: Mutual interaction of soil moisture state and atmospheric processes. *J. Hydrol.,* **184,** 3–17.

Erfani, A., A. Methot, R. Goodson, S. Belair, K. S. Yeh, J. Cote, and R. Moffet, 2003: Synoptic and mesoscale study of a severe convective outbreak with the nonhydrostatic Global Environmental Multiscale (GEM) model. *Meteor. Atmos. Phys.,* **82,** 31–53.

——, J. Mailhot, S. Gravel, M. Desgagné, P. King, D. Sills, N. McLennan, and D. Jacob, 2005: The

high resolution limited area version of the Global Environmental Multiscale model and its potential operational applications. Preprints, *11th Conf. on Mesoscale Processes,* Albuquerque, NM, Amer. Meteor. Soc., 1M.4. [Available online at http://ams.confex.com/ams/32Rad11Meso/techprogram/paper_97308.htm.]

Fillion, L., and Coauthors, 2010: The Canadian regional data assimilation and forecasting system. *Wea. Forecasting,* **25,** 1645–1669.

Fouquart, Y., and B. Bonnel, 1980: Computations of solar heating of the earth's atmosphere: A new parameterization. *Contrib. Atmos. Phys.,* **53,** 35–62.

Garand, L., and J. Mailhot, 1990: The influences of infrared radiation on numerical weather forecasts. Preprints, *Seventh Conf. on Atmospheric Radiation,* San Francisco, CA, Amer. Meteor. Soc., J146–J151.

Hanesiak, J. M., R. L. Raddatz, and S. Lobban, 2004: Local initiation of deep convection on the Canadian prairie provinces. *Bound.-Layer Meteor.,* **110,** 455–470.

Hill, L. M., 2006: Drylines observed in Alberta during A-GAME. M.S. thesis, Dept. of Earth and Atmospheric Sciences, University of Alberta, 111 pp.

Honch, R. W., and G. S. Strong, 1990: Mesoscale dynamics associated with convection during LIMEX-85. Preprints, *16th Conf. on Severe Local Storms,* Kananaskis Park, AB, Canada, Amer. Meteor. Soc., 681–686.

Houston, A. L., and D. Niyogi, 2007: The sensitivity of convective initiation to the lapse rate of the active cloud-bearing layer. *Mon. Wea. Rev.,* **135,** 3013–3032.

King, P. and D. M. L. Sills, 1998: The 1997 ELBOW Project: an experiment to study the Effects of Lake Breezes on Weather in southern Ontario. Preprints, *19th Conf. on Severe Local Storms,* Minneapolis, MN, Amer. Meteor. Soc., 317–320.

——, M. J. Leduc, D. M. L. Sills, N. R. Donaldson, D. R. Hudak, P. Joe, and B. P. Murphy, 2003: Lake breezes in southern Ontario and their relation to tornado climatology. *Wea. Forecasting,* **18,** 795–807.

Kingsmill, D. E., 1995: Convection initiation associated with a sea-breeze front, a gust front, and their collision. *Mon. Wea. Rev.,* **123,** 2913–2933.

Knott, S. R. J., and N. M. Taylor, 2000: Operational aspects of the Alberta severe weather outbreak of 29 July 1993. *Natl. Wea. Dig.,* **24,** 11–23.

Lemone, M. A., F. Chen, J. G. Alfieri, M. Tewari, B. Geerts, Q. Miao, R. L. Grossman, and R. L. Coulter, 2007: Influence of land cover and soil moisture on the horizontal distribution of sensible and latent heat fluxes in southeast Kansas during IHOP_2002 and CASES-97. *J. Hydrometeor.,* **8,** 68–87.

Longley, R. W., and C. E. Thompson, 1965: A study of the causes of hail. *J. Appl. Meteor.,* **4,** 69–82.

Mailhot, J., and Coauthors, 2010: Environment Canada's experimental numerical weather prediction systems for the Vancouver 2010 Winter Olympic and Paralympic Games. *Bull. Amer. Meteor. Soc.,* **91,** 1073–1085.

McCaul, E. W., and C. Cohen, 2002: The impact on simulated storm structure and intensity of variations in the mixed layer and moist layer depths. *Mon. Wea. Rev.,* **130,** 1722–1748.

McDonald, M., 2009: 2009 prairie summer severe weather event climatology and verification results report. Meteorological Service of Canada Internal Rep., 32 pp.

McTaggart-Cowan, R., T. J. Galarneau Jr., L. F. Bosart, and J. A. Milbrandt, 2010: Development and tropical transition of an alpine lee cyclone. Part II: Orographic influence on the development pathway. *Mon. Wea. Rev.,* **138,** 2308–2326.

Milbrandt, J. A., and M. K. Yau, 2005: A multimoment bulk microphysics parameterization. Part II: A proposed three-moment closure and scheme description. *J. Atmos. Sci.,* **62,** 3065–3081.

——, and ——, 2006a: A multimoment bulk microphysics parameterization. Part III: Control simulation of a hailstorm. *J. Atmos. Sci.,* **63,** 3114–3136.

——, and ——, 2006b: A multimoment bulk microphysics parameterization. Part IV: Sensitivity experiments. *J. Atmos. Sci.,* **63,** 3137–3159.

Mueller, C. K., J. W. Wilson, and N. A. Crook, 1993: The utility of sounding and mesonet data to nowcast thunderstorm initiation. *Wea. Forecasting,* **8,** 132–146.

Pielke, R. A., Sr., 2001: Influence of the spatial distribution of vegetation and soils on the prediction of cumulus convective rainfall. *Rev. Geophys.,* **39,** 151–177.

Raddatz, R. L., 1998: Anthropogenic vegetation transformation and the potential for deep convection on the Canadian prairies. *Can. J. Soil Sci.,* **78,** 656–666.

——, 2000: Summer rainfall recycling for an agricultural region of the Canadian prairies. *Can. J. Soil Sci.,* **80,** 367–373.

——, 2005: Moisture recycling on the Canadian prairies for summer droughts and pluvials from 1997 to 2003. *Agric. For. Meteor.,* **131,** 13–26.

——, and J. D. Cummine, 2003: Inter-annual variability of moisture flux from the prairie agro-ecosystem: Impact of crop phenology on the seasonal pattern of tornado days. *Bound.-Layer Meteor.,* **106,** 283–295.

——, and M. Noonan, 2004: Monthly mean afternoon mixing-layer depths "tuned" to the eco-climatic regions of the Canadian prairie provinces. *Environ. Model. Assess.,* **9,** 147–158.

Renick, J. H., and J. B. Maxwell, 1977: Forecasting hailfall in Alberta. *Hail: A Review of Hail Science and Hail Suppression, Meteor. Monogr.,* No. 38, Amer. Meteor. Soc., 145–151.

Sills, D., P. Taylor, P. King, W. Hocking, and I. Nichols, 2002: ELBOW 2001—Studying the relationship between lake breezes and severe weather: Project overview and preliminary results. Preprints, *21st Conf. on Severe Local Storms,* San Antonio, TX, Amer. Meteor. Soc., 611–614.

——, M. L., J. W. Wilson, P. I. Joe, D. W. Burgess, R. M. Webb, and N. I. Fox, 2004: The 3 November tornadic event during Sydney 2000: Storm evolution and the role of low-level boundaries. *Wea. Forecasting,* **19,** 22–42.

Smith, S. B., and M. K. Yau, 1993a: The causes of severe convective outbreaks in Alberta. Part I: A comparison of a severe outbreak with two nonsevere events. *Mon. Wea. Rev.,* **121,** 1099–1125.

——, and ——, 1993b: The causes of severe convective outbreaks in Alberta. Part II: Conceptual model and statistical analysis. *Mon. Wea. Rev.,* **121,** 1126–1133.

Statistics Canada, cited 2007: Population and dwelling counts: A portrait of the Canadian population. [Available online at http://www12.statcan.ca/census-recensement/2006/rt-td/pd-pl-eng.cfm.]

Stensrud, D. J., and Coauthors, 2009: Convective-scale warn-on-forecast system—A vision for 2020. *Bull. Amer. Meteor. Soc.,* **90,** 1487–1499.

Strong, G. S., 1986: Synoptic to mesoscale dynamics of severe thunderstorm environments: A diagnostic study with forecasting implications. Ph.D. thesis, University of Alberta, 345 pp.

——, 1989: LIMEX-85: Processing of data sets from an Alberta mesoscale upper-air experiment. *Climatol. Bull.,* **23,** 98–118.

——, 1997: Atmospheric moisture budget estimates of regional evapotranspiration from RES-91. *Atmos.–Ocean,* **35,** 29–63.

Taylor, N. M., 1999: Climatology of convective sounding parameters identifying the potential for convective storm development over central Alberta. M.S. thesis, Dept. of Earth and Atmospheric Sciences, University of Alberta, 121 pp.

——, D. Sills, J. Hanesiak, J. Milbrandt, C. Smith, P. McCarthy, and G. Strong, 2007: The Understanding Severe Thunderstorms and Alberta Boundary Layers Experiment: UNSTABLE; Scientific overview. Environment Canada Rep., 84 pp. [Available online at www.umanitoba.ca/faculties/environment/envirogeog/weather/unstable/UNSTABLE_Science_Final.pdf.]

——, ——, ——, ——, ——, G. Strong, S. Skone, and P. McCarthy, 2008a: The Understanding Severe Thunderstorms and Alberta Boundary Layers Experiment: 2008 pilot experiment operations plan. Environment Canada Rep., 58 pp. [Available online at www.umanitoba.ca/environment/envirogeog/weather/unstable/Operations/2008_OpsPlan_Final.pdf.]

——, and Coauthors, 2008b: The Understanding Severe Thunderstorms and Alberta Boundary Layers Experiment (UNSTABLE): Overview and preliminary results. Preprints, *24th Conf. on Severe Local Storms,* Savannah, GA, Amer. Meteor. Soc., 18.7. [Available online at http://ams.confex.com/ams/24SLS/techprogram/paper_142207.htm.]

Trier, S. B., F. Chen, and K. W. Manning, 2004: A study of convection initiation in a mesoscale model using high-resolution land surface initial conditions. *Mon. Wea. Rev.,* **132,** 2954–2976.

Weaver, C. P., and R. Avissar, 2001: Atmospheric disturbances caused by human modification of the landscape. *Bull. Amer. Meteor. Soc.,* **82,** 269–281.

Weckwerth, T. M., 2000: The effect of small-scale moisture variability on thunderstorm initiation. *Mon. Wea. Rev.,* **128,** 4017–4030.

——, and R. M. Wakimoto, 1992: The initiation and organization of convective cells atop a cold-air outflow boundary. *Mon. Wea. Rev.,* **120,** 2169–2187.

——, and D. B. Parsons, 2006: A review of convection initiation and motivation for IHOP_2002. *Mon. Wea. Rev.,* **134,** 5–22.

——, J. W. Wilson, and R. M. Wakimoto, 1996: Thermodynamic variability within the convective boundary layer due to horizontal convective rolls. *Mon. Wea. Rev.,* **124,** 769–784.

——, D. B. Parsons, S. E. Koch, J. A. Moore, M. A. LeMone, B. B. Demoz, C. Flamant, B. Geerts, J. Wang, and W. F. Feltz, 2004: An overview of the International H20 Project (IHOP_2002) and some preliminary highlights. *Bull. Amer. Meteor. Soc.,* **85,** 253–277.

Wilson, J. W., and W. E. Schreiber, 1986: Initiation of convective storms at radar-observed ABL convergence lines. *Mon. Wea. Rev.,* **114,** 2516–2536.

——, and C. K. Mueller, 1993: Nowcasts of thunderstorm initiation and evolution. *Wea. Forecasting,* **8,** 113–131.

——, and R. D. Roberts, 2006: Summary of convective storm initiation and evolution during IHOP: Observational and modeling perspective. *Mon. Wea. Rev.,* **134,** 23–47.

Wojtiw, L., 1975: Climatic summaries of hailfall in central Alberta (1957–1973). Alberta Research Atmospheric Science Rep. 75-1, 102 pp.

Wulfmeyer, V., and Coauthors, 2008: RESEARCH CAMPAIGN: The Convective and Orographically Induced Precipitation Study. *Bull. Amer. Meteor. Soc.,* **89,** 1477–1486.